NACA RM L56C05

RM L56C05

NACA

RESEARCH MEMORANDUM

TURBULENT AND LAMINAR HEAT-TRANSFER MEASUREMENTS ON A 1/6-SCALE NACA RM-10 MISSILE IN FREE FLIGHT TO A MACH NUMBER OF 4.2 AND TO A WALL TEMPERATURE OF 1400° R

By Robert O. Piland, Katherine A. Collie,
and William E. Stoney

Langley Aeronautical Laboratory
Langley Field, Va.

NATIONAL ADVISORY COMMITTEE
FOR AERONAUTICS

WASHINGTON
July 3, 1956
Declassified July 22, 1959

NACA RM L56C05

NATIONAL ADVISORY COMMITTEE FOR AERONAUTICS

RESEARCH MEMORANDUM

TURBULENT AND LAMINAR HEAT-TRANSFER MEASUREMENTS ON A 1/6-SCALE NACA RM-10 MISSILE IN FREE FLIGHT TO A MACH NUMBER OF 4.2 AND TO A WALL TEMPERATURE OF 1400° R

By Robert O. Piland, Katherine A. Collie,
and William E. Stoney

SUMMARY

Aerodynamic-heating data were obtained between Mach numbers of 1.2 and 4.2 from a free-flight test of a 1/6-scale finless NACA RM-10. Transient skin temperatures were measured at six stations along the body. The maximum skin temperature recorded during flight was 1400° R. The test of Reynolds number covered a range from 4.2×10^6 to 27.0×10^6.

Temperature recovery factors were obtained for each station at a single time during the flight. The values agreed with Prandtl number to the one-third power within ±3 percent.

The experimental turbulent Stanton numbers were in fair agreement with Van Driest's theory (assuming transition at the tip) during the time the skin was heating. During the skin-cooling period that followed, the experimental values were consistently higher than the theoretical.

During the skin-heating period as turbulent heat-transfer coefficients were being measured, a sudden "burst" of laminar flow occurred for 0.5 second. The laminar or transitional flow extended to 38 percent of the body length or a Reynolds number of 13.3×10^6. For a short time prior to, during, and after the "burst," the Mach number and heating conditions were such that the two-dimensional stability theorem would have predicted the possibility of an infinite length of laminar flow. At one other very short period of time while the model was in the stability region, there was no evidence of laminar flow.

Laminar heat-transfer coefficients were measured again during the latter part of the test. Transition from turbulent to laminar flow

began at local Reynolds numbers of 3 to 4 $\times 10^6$. Poor agreement was obtained with laminar theory at the foremost station. The agreement became progressively better moving rearward on the body.

INTRODUCTION

Reference 1 presented drag data from a free-flight test of a 1/6-scale, sting-mounted NACA RM-10 model. In assessing these data, it appeared as if transition might have occurred during the flight. Full-scale RM-10 heat-transfer models which allow assessment of the condition of the boundary layer (refs. 2 and 3) had previously been tested over this Mach number range (1.0 to 4.0) but at much higher Reynolds numbers and no evidence of transition or laminar flow was noted. Because of the need for information on transition and heating data at all Reynolds numbers, it was decided to test a similar 1/6-scale RM-10 instrumented to measure skin temperature at stations along the model; these temperature data, when reduced to heat-transfer coefficients, would indicate by their magnitude the nature of the boundary layer.

The heating data obtained from this flight are therefore reported herein for a Mach number range of 1.2 to 4.2 and a Reynolds number range of 4.2 $\times 10^6$ to 27.0 $\times 10^6$. The maximum skin temperature recorded during the flight was 1400° R. The test was conducted at the Langley Pilotless Aircraft Research Station at Wallops Island, Va., in January 1955.

SYMBOLS

Q	quantity of heat, Btu
A	area, sq ft
h	local aerodynamic heat-transfer coefficient, Btu/sec-sq ft-$^\circ$F
T	temperature
ϵ	emissivity
σ_b	Stefan-Boltzman constant, 0.4835 $\times 10^{-12}$, Btu/ft^2-sec-$^\circ$R^4
k	thermal conductivity of air, Btu-ft/sec-$^\circ$F-sq ft

k_W thermal conductivity of Inconel, Btu-ft/sec-^oF-sq ft

τ_W thickness, ft

ρ_W specific weight of wall, lb/ft^3

c_W specific heat of wall material, Btu/lb-^oF

C_H Stanton number

c_p specific heat of air at constant pressure, Btu/slug-^oF

ρ density of air, slugs/cu ft

V velocity, ft/sec

γ ratio of specific heats

p pressure, lb/sq ft

R gas constant for air, 1716 ft^2/sec^2-^oR

A,B constants in approximate equation for c_W

R.F. recovery factor, $\frac{T_{aw} - T_v}{T_{so} - T_v}$

Pr Prandtl number

J mechanical equivalent of heat

g standard acceleration of gravity

M Mach number

R Reynolds number, $\frac{\rho V x}{\mu}$

μ viscosity of air, slugs/ft-sec

t time from start of flight, sec

x axial distance along body from the nose, ft

σ standard deviation (with subscripts to indicate quantity involved)

σ_{C_H} maximum probable error in C_H

Subscripts:

aw adiabatic wall

o undisturbed free stream ahead of model

so stagnation

v just outside boundary layer

w wall (skin)

s sting

MODEL, INSTRUMENTATION, AND TEST

The test model was a 1/6-scale, finless NACA RM-10, sting mounted on a carrier body which housed the instrumentation and sustainer rocket motor. A photograph of the test model is shown in figure 1. A sketch of the test model and the carrier body is presented on figure 2. The model skin was formed by spinning a 1/32-inch-thick sheet of Inconel, then highly polished. The skin-thickness measurements were made on the finished model by using micrometers. The surface roughness was of the order of 10 microinches. There was a break in the model at station 15 for purpose of assembly. Shortly behind the break there was a circumferential row of flat-head screws.

Skin-temperature measurements were made at six stations along the body as shown in figure 2(b) by use of thermocouples. The thermocouple wire was no. 30 chromel-alumel. The junction between the wires consisted of a bead of about 0.01 inch in diameter, formed by fusing the wires together and using the mercury-bath technique. Care was taken that the wires were not in contact except within the bead. The beads were fitted into holes drilled through the Inconel skin at the proper stations, with the thermocouple leads inside the nose. The holes were then welded closed with Inconel welding rod and the exterior surface was smoothed and polished. The cold junctions of the thermocouples were potted in paraplex inside of a brass block of sufficient mass that no change in cold-junction temperature would occur during the relatively short time of the test. The cold-junction temperature was measured just prior to launching by a resistance-type temperature pickup also potted inside the brass block. A cross check of this temperature was obtained by

simultaneously measuring the skin temperature with a thermocouple taped to the exterior surface of the nose.

During flight, three standard voltages and the outputs of the six thermocouples were commutated and transmitted on a single telemeter channel. The commutation rate and the electronic system were such that each thermocouple voltage was transmitted 14 times per second, and each standard voltage was transmitted 7 times per second. The three standard voltages, supplied by a mercury cell and a voltage-divider network, were chosen equivalent to the lowest temperature, the midrange temperature, and the highest temperature that the skin thermocouples were expected to reach. Commutation and transmission of these known voltages along with the voltage readings of the skin thermocouples provided an in-flight check calibration of the thermocouple telemeter and recording system.

The sustainer rocket motor was a 6.25-inch ABL Deacon rocket motor. The booster consisted of a cluster of three of these rockets. The model and booster on the launcher are shown in figure 3.

The model was launched at an angle of 70° to the horizontal. The booster propelled the model to a Mach number of 2.2. After a 1-second coasting period, the sustainer motor fired and accelerated the model to a peak Mach number of 4.2.

During the time of rocket-motor firing and the coasting period that followed, an NACA telemeter located in the carrier body was relaying the temperature measurements to ground-receiving stations. The model velocity was measured by CW Doppler radar, and SCR 584 tracking radar measured the flight path, giving horizontal range, altitude, and flight-path angle. Atmospheric conditions were measured by radiosondes, one launched some time prior to flight to reach high altitude by the time the model was fired, and one at the time the model was launched to accurately measure low-altitude data. Although no instrumentation was carried in the model to make a direct measurement of angle of attack, the size of the stabilizing fins was such as to make the carrier body a highly stable vehicle so that an angle of attack near zero ($\pm 1^{\circ}$) was maintained. Measurements such as flight path or static pressure (not presented herein) gave no indication that the model followed other than a zero-lift trajectory.

DATA REDUCTION

During the flight test of the model, the following information was obtained as a function of flight time:

(1) Skin temperature measurements (fig. 4)

(2) Model velocity, Mach number, and altitude (fig. 5)

(3) Air properties at any given time (density, static temperature, and speed of sound)

It is desirable to reduce this information into the form of Stanton number and recovery factors. The method of reduction used is described in the following sections:

Stanton Number

The basic heat-transfer equations as given in reference 4 are:

For convection:

$$\frac{dQ_1}{dt} = h\left(T_{aw} - T_w\right)A \tag{1}$$

For radiation outward:

$$\frac{dQ_2}{dt} = \epsilon\sigma_b T_w^{\,4} A \tag{2}$$

For radiation inward (model skin to internal sting):

$$\frac{dQ_3}{dt} = \sigma_b\left[\frac{1}{\frac{A_w}{A_s}\left(\frac{1}{\epsilon_s}\right) + \frac{1}{\epsilon_w} - 1}\right]\left(T_w^{\,4} - T_s^{\,4}\right)A \tag{3}$$

For conduction longitudinally through skin:

$$\frac{dQ_4}{dt} = k_w \tau_w \frac{\partial^2 T}{\partial x^2} A \tag{4}$$

Equations (3) and (4) are strictly applicable for the case of two coaxial cylinders and a cylinder, respectively. Since the model shape in the present case is parabolic, the equations are approximations. The error introduced in the heat-transfer coefficients by these approximations is discussed in the section "Accuracy of Stanton Numbers."

The time rate of change of heat contained in the skin is

$$\frac{dQ}{dt} = \rho_w \tau_w c_w \frac{dT_w}{dt} A \tag{5}$$

The summation of the quantities of heat contributed by convection, radiation, and conduction (eqs. (1), (2), (3), (4)) will equal the heat contained in the skin (eq. (5)). Neglect conduction, which is less than 1 percent of the total heat transfer, and cancel A throughout; then

$$\rho_w \tau_w c_w \frac{dT_w}{dt} = h\left(T_{aw} - T_w\right) - \epsilon \sigma_b T_w^4 - \sigma_b \left[\frac{1}{\frac{A_w}{A_s}\left(\frac{1}{\epsilon_s}\right) + \frac{1}{\epsilon_w} - 1}\right]\left(T_w^4 - T_s^4\right)$$

therefore

$$h = \frac{\rho_w \tau_w c_w \frac{dT_w}{dt} + \epsilon \sigma_b T_w^4 + \sigma_b \left[\frac{1}{\frac{A_w}{A_s}\left(\frac{1}{\epsilon_s}\right) + \frac{1}{\epsilon_w} - 1}\right]\left(T_w^4 - T_s^4\right)}{\left(T_{aw} - T_w\right)} \tag{6}$$

From the local convective heat-transfer coefficient (eq. (6)), the Stanton number can be determined:

$$C_H = \frac{h}{c_{p,v} \rho_v V_v} \tag{7}$$

The properties of the test material (Inconel) are known. The thickness τ_w was measured with micrometers at the various stations and was between 0.031 and 0.033 inch. The density ρ_w is constant. The specific heat c_w varies with skin temperature, as shown on figure 6. These data were measured by the National Bureau of Standards and are presented in reference 5. The emissivity of the material is considered to be 0.3 throughout the flight. Measurements in reference 5 show that for nonoxidized Inconel, the emissivity varies only slightly from the value of 0.3 for the temperature range of the test. The rate of change of temperature with time dT/dt was mechanically read, using the measured temperature data. The sting temperature T_s used in

calculating the radiation term was assumed to be constant and equal to ground air temperature. The thermodynamic properties of air (c_p, Pr, etc.) used in the computations were obtained from reference 6 and are presented in figure 7. The adiabatic wall temperature T_{aw} was obtained from the definition of recovery factor (ref. 3):

$$R.F. = \frac{T_{aw} - T_v}{T_{so} - T_v}$$

This leads to

$$T_{aw} = T_v + Pr^{1/3}\left(T_{so} - T_v\right)$$

The turbulent recovery factor is taken equal to $Pr^{1/3}$ and the laminar recovery factor is taken equal to $Pr^{1/2}$, both based on wall temperature. The turbulent recovery factor was assumed equal to $Pr^{1/3}$ because $Pr^{1/3}$ has been shown to approximate the measured recovery factor within one percent for a variety of test conditions. (See ref. 7.) The measured recovery factors were not used since they were obtained at only one time during the flight and hence at only one temperature condition. The laminar recovery factor was assumed equal to $Pr^{1/2}$, which is also a reasonable approximation as shown by reference 7. The stagnation temperature was computed from the energy equation

$$\frac{V^2}{2Jg} = \int_{T_o}^{T_{so}} c_p \, dT$$

which takes into account the variation of the specific heat of air with temperature. Figure 8 gives a typical time history of adiabatic, stagnation, and skin temperatures. The temperature T_o is known from model altitude and radiosonde measurements. The local temperature just outside the boundary layer T_v is obtained by correcting the free-stream temperature T_o for the effect of body pressures at the various stations. The slender-body theory of Jones and Margolis (ref. 8) was used for calculating the pressure distribution at supersonic speeds. Local values of velocity and density were also obtained for use in reducing the local convective heat-transfer coefficients h to Stanton numbers $\left(C_H = \frac{h}{c_{p,v}\rho_v V_v}\right)$.

Recovery Factor

Recovery factors were determined at each temperature measuring station at a single time during the flight by using the following method.

If the convective heat transfer is assumed to be zero, equation (6) may be rewritten

$$\frac{dT_w}{dt} = -\left[\frac{\epsilon_w \sigma_b T_w^4 + \sigma_b\left[\frac{1}{\frac{1}{\epsilon_w} + \frac{A_w}{A_s}\frac{1}{\epsilon_s} - 1}\right] T_w^4 - T_s^4}{\rho_w \tau_w c_w}\right]$$

By a cut-and-try process, the slope dT/dt which satisfied the conditions on the right-hand side of the equation was found. The time corresponding to this slope will be the time of zero convective heat transfer. Now at the time of zero convective heat transfer, the temperature of the wall T_w will equal the adiabatic wall temperature T_{aw}. Therefore, at this given time we may determine a recovery factor, since

$$R.F. = \frac{T_{aw} - T_v}{T_{so} - T_v}$$

Accuracy of Stanton Numbers

The accuracy of the Stanton numbers is dependent upon the possible errors in the various measured and estimated quantities used in equations (6) and (7). An appendix is devoted to a discussion of these errors and their probable resulting errors in C_H. Before discussing these more specific sources of error, let us consider the applicability of the equations used in determining C_H. Equation (3) is strictly applicable for two coaxial cylinders whereas in the present case the model is parabolic in shape. In order to estimate roughly the order of magnitude of error that might be expected from this approximation, the relative contributions of convective and radiative heat transfer were determined. Figure 9 presents the variation of h with time for a typical station indicating the relative magnitude of the convective and radiative heat transfer. It is seen that the total radiative heat transfer is at most 20 percent of the total. Furthermore, the radiative heat transfer inward, not shown on the figure, was at the most only 1.5 percent of the total heat transfer. Consequently, even if the use

of equation (3) results in a fairly large percentage error in the calculation of the inward radiative heat transfer, the error contributed to h would still be small.

Equation (4) is strictly applicable for the case of conduction longitudinally through a cylinder. The heat transfer for the present parabolic case calculated from equation (4) was a negligible part of the total heat transfer. In addition, the longitudinal conduction through a conical skin was calculated and this contribution to the total was also negligible.

Using the method presented in the appendix, the errors in C_H attributable to errors in the various measured and estimated quantities of equations (6) and (7) have been calculated for station 6. The measured value of C_H, together with an accuracy band, are presented in figure 10 as a function of time. The ratio of the probable error in C_H to the experimentally determined C_H, plotted as σ_{C_H}/C_H, is also presented in this figure. It can be seen that the accuracy of C_H varies greatly during the test and this is primarily due to the variation of $T_{aw} - T_w$. (See fig. 10.) The greater the magnitude of this quantity, the greater is the accuracy of the values of C_H; and conversely, as $T_{aw} - T_w$ approaches zero, the inaccuracy of C_H becomes so great that the data are of no value. The data presented in this report, therefore, include only those which are accurate within 20 percent. The accuracy band and ratio σ_{C_H}/C_H presented in figure 10 are strictly applicable to the data at station 6. However, at the other temperature measuring stations the accuracy of C_H at any given time is essentially the same as the accuracy of the data at station 6.

RESULTS AND DISCUSSION

Experimental Recovery Factors

The recovery factors determined as described previously are presented in figure 11 as a function of model station. It should be noted that the recovery factors were evaluated at different times at different stations. The theoretical values of recovery factor $Pr^{1/3}$ and $Pr^{1/2}$, based on the wall temperature at the times the recovery factors were determined, are also presented. The experimental values are seen to agree with $Pr^{1/3}$ within ±3 percent for all stations. Consequently, a turbulent boundary layer is indicated at all stations at the time for which the recovery factors were computed.

Stanton Number

The experimental and theoretical (Van Driest, refs. 9 and 10) Stanton numbers are presented in figure 12 as a function of flight time for six temperature measuring stations. The parameters R_V, M_V, and T_W/T_V, which theoretically determine C_H, are also presented on figure 12 as a function of time. For all six stations the theoretical variation of C_H with time is presented. These calculations are obtained by using conical theory and assuming turbulent flow to exist from the nose tip. The theoretical flat-plate values have been modified in accordance with references 11 and 12 to give the proper value for a conical shape. The test model, although not a cone, is more nearly approximated by the cone than by the flat plate, at least at the forward stations. In addition, at the most forward station a theoretical curve is presented where conical theory is again used and transition is assumed to occur at a Reynolds number of 2×10^6. At the most rearward station a theoretical curve is also presented where calculations are based on flat-plate theory.

It should be kept in mind that the theories of Van Driest with which the experimental data are compared were developed on the assumption of a constant wall temperature and constant pressure distribution. As can be seen in figure 4 there is considerable variation of temperature along the body at any given time. The pressures also along the body are not constant, the body being neither a flat plate nor a cone. The effect of the pressure gradient is taken into account in obtaining the Stanton numbers by using values of density and velocity just outside the boundary layer.

Consider first the data obtained while the skin is being heated. These data cover the period of accelerating flight and a small portion of decelerating flight and extend to a time about 10 seconds after take-off. Except for a short period of time between 5.5 and 6.0 seconds, the experimental Stanton numbers (fig. 12) are in fair agreement with the turbulent theory results obtained by assuming transition at the nose tip. From station to station the agreement varies somewhat, but no significant consistent trends away from the theory are noted. At station 6 the theoretical values of C_H obtained on the assumption of transition at a Reynolds number of 2×10^6 do not differ greatly from those obtained on the assumption of transition at the nose tip. Up to about 8 seconds after take-off the experimental data are in better agreement with the theory based on the assumption of transition at the nose tip. Between 8 and 10 seconds after take-off the agreement is better if a transition Reynolds number of 2×10^6 is assumed.

At 5.5 seconds after take-off at stations 6, 7.7, and 9.4, with the local Reynolds number varying from 4×10^6 to 6.5×10^6, the Stanton

numbers dropped to the theoretical laminar level. This result must have been due to a sudden "burst" of laminar flow. The effect was most pronounced at station 6 and decreased at the more rearward stations. No effect can be seen at station 11.1. In an effort to determine the cause of the laminar burst, recourse was made to the two-dimensional laminar boundary-layer stability theory of reference 13. Figure 13 presents a region defined by values of temperature ratio T_w/T_v and Mach number in which, theoretically, infinite stability of the laminar boundary layer is attainable. The flight data show the model to have been in this region twice, between Mach numbers 1.5 and 2.0 and between Mach numbers 2.5 and 3.8. It was during the second period in the stability region that the burst occurred, as shown in this figure.

Between about 10 and 12 seconds after take-off, the skin temperatures reach maximums and the forcing function $T_{aw} - T_w$ passes through zero. As discussed in the section entitled "Accuracy of Stanton Numbers," this phenomenon results in inaccuracies in C_H large enough to make data in this interval meaningless and they therefore are not presented.

After about 12 seconds after take-off the model is decelerating, and Mach number, Reynolds number, and wall temperatures are decreasing. The measured Stanton numbers are seen to be consistently and considerably higher than values predicted by turbulent theory (transition at nose tip) until the time when transition to laminar flow begins (approx. 15 sec). For a possible explanation refer to figure 12(a) which presents the data obtained at station 6. It can be seen that in this time interval the experimental data are in fair agreement with the theoretical values when transition is assumed at a Reynolds number of 2×10^6. Since transition occurs shortly afterward at Reynolds numbers of about 3×10^6, this explanation of the seeming disagreement is likely. It should also be kept in mind that the accuracy of the data in this time interval is about ±12 percent which could account for a part of the disagreement.

Transition is seen to begin at a Reynolds number of 3 to 4×10^6 at about 15 seconds. Laminar heat-transfer coefficients are obtained as far rearward as station 11.1 (figs. 12(a) to 12(d)). Station 12.8 (fig. 12(e)) shows the beginning of transition, but a laminar level had not been reached at the latest time (20 sec) for which data are available. The laminar coefficients at station 6 are not in good agreement with the laminar theory. At the more rearward stations, fair agreement is obtained. The possibility exists that the distribution of temperature along the nose, forward of station 6, is of such a nonuniform nature due to the particular construction of the model as to affect the measured laminar Stanton numbers. At more rearward stations on the body the nonuniform temperature near the nose tip would probably have less effect.

Figure 14 presents the variation of Stanton number with station in inches from the nose tip at various times during the flight. At the time of 1.8 seconds, the measured Stanton numbers are lower than the turbulent theory. Possible inaccuracies in the data at this time could account for most of the disagreement. At the time of 4.2 seconds the agreement with theory is good. At the time of 5.8 seconds the typical laminar, transition, turbulent curve is obtained. This time corresponds to the time of measuring the lowest heat-transfer coefficients during the laminar burst. At 7.0 and 9.0 seconds, the data are again in good agreement with turbulent theory. At 14.0 seconds, during skin cooling, the poor agreement discussed previously is obtained.

Assuming a Reynolds number of transition of 2×10^6 improves the agreement, especially at station 6, as has been previously discussed. At the more rearward stations, however, the agreement is not improved significantly. At 18 seconds the variation of C_H with station indicates the laminar, transition, and turbulent regions. The laminar coefficients, however, are considerably higher than the theoretical laminar values and the turbulent value at station 18 is somewhat higher than turbulent theory. At 20 seconds the laminar coefficients, with the exception of station 6, are in fair agreement with the theory. As stated earlier, in considering the laminar coefficients it should be remembered that the theory used here was developed on the assumption of a constant temperature ahead of the measuring station.

CONCLUDING REMARKS

An NACA RM-10 1/6-scale model has been flight-tested and convective heat-transfer coefficients (Stanton numbers) have been obtained at six stations along the body. The Mach number range was from 1.2 to 4.2 and the Reynolds number range was from 4.2×10^6 to 27.5×10^6. The maximum recorded temperature was 1400° R. The following observations have been made from a comparison of experiment and theory:

1. The Stanton numbers predicted by the turbulent theory of Van Driest (on the assumption of transition at the nose tip) were in good agreement with experiment during the period when the skin was being heated. During the cooling period that followed, the measured Stanton numbers were consistently higher than theory.

2. The measured recovery factors obtained at each station at a single time during the flight agreed with Prandtl number to the 1/3 power within ±3 percent, indicating that turbulent flow existed at the time at which recovery factors were determined.

3. A sudden "burst" of laminar flow occurred at a Mach number of 2.9 and extended to 38 percent of the body length corresponding to a Reynolds number of 13.3×10^6. The model at this time was in the theoretical region of infinite stability of the laminar boundary layer.

4. Transition from turbulent flow begins toward the end of the test when the Reynolds number has dropped to 3 to 4×10^6. At this time the model was well out of the region of laminar boundary-layer stability.

Langley Aeronautical Laboratory,
National Advisory Committee for Aeronautics,
Langley Field, Va., February 16, 1956.

APPENDIX A

ESTIMATED ERRORS

By William E. Stoney

Accuracy of C_H

Errors may be grouped under two headings, systematic and random. (This discussion follows the treatment in ref. 14.) Random errors are those which in a large number of measurements are as often negative as positive, and thus they affect the arithmetic mean but little. All other errors are classed as systematic.

Systematic errors can be evaluated only by comparison of the final data with previously substantiated results, either theoretical or empirical. Although the number of previous tests with which such comparisons can be made is not large, such comparisons have indicated that there has been little or no systematic error present and such will be assumed in the present case.

Random errors appear in all the measured quantities. These individual errors will be quoted as standard deviations (σ), that is, the root mean square of the deviations of a set of observations from its mean value. In general, these values will be estimated from what are, statistically speaking, small samples and are thus themselves approximate in nature. The effect of the individual values of σ on C_H will be presented in the form

$$\frac{\sigma_{C_H}}{C_H} = \left| \frac{\partial C_H}{\partial x} \frac{\sigma_x}{C_H} \right|$$

As the individual errors act independently of one another, their combined effect on C_H will be given by the following equation:

$$\frac{\sigma_{C_{H_{total}}}}{C_H} = \left(\sum_{x=a}^{z} \left(\frac{\sigma_{C_H}}{C_H} \right)_x^2 \right)^{1/2} \tag{A1}$$

The equation for C_H reduced to the quantities which are measured, calculated, or assumed is presented below:

$$C_H = \frac{\rho_w \tau_w \left(A_w + BT_w\right)\frac{dT_w}{dt} + \sigma_b \epsilon_w T_w^4 + \sigma_b \left(\frac{T_w^4 - T_s^4}{\frac{1}{\epsilon_w} + \frac{A_w}{A_s}\frac{1}{\epsilon_s} - 1}\right)}{\rho_o \left(\frac{\rho_v}{\rho_o}\right) V_o \left(\frac{V_v}{V_o}\right) c_{p,v} \left\{ R.F. \left[T_o \left(1 + \frac{0.2V_o^2}{\gamma R T_o}\right) - \left(\frac{T_v}{T_o}\right) T_o \right] + \left(\frac{T_v}{T_o}\right) T_o - T_w \right\}} \tag{A2}$$

where the approximate expression $(A + BT_w)$ has been substituted for c_w. In the actual data reduction, experimental values of c_w were used. Also, the approximation $\left(1 + \frac{0.2V_o^2}{\gamma R T_o}\right)$ has been substituted for the equation

$$\frac{V^2}{2Jg} = \int_{T_o}^{T_{so}} c_p \, dT$$

which was used to get T_{so} in the text. Equation (A2) will be referred to ocasionally in its more compact form:

$$C_H = \frac{\rho_w \tau_w c_w \frac{dT_w}{dt} + r}{\rho_v V_v c_{p,v} \left(T_{aw} - T_w\right)}$$

where r refers to the radiation terms.

The equations for $\frac{\sigma C_H}{C_H}$ due to the errors in the individual quantities are presented below. The expressions for those quantities which have been assumed or which have negligible effect on the accuracy of C_H have been omitted.

Quantity	$\frac{\sigma_{C_H}}{C_H}$ due to σ
T_w	$\left\lvert \left\{ \frac{\rho_w \tau_w \frac{dT_w}{dt} B + 4\sigma_b T_w^3 \left[\epsilon_w + \frac{1}{\left(\frac{1}{\epsilon_w} + \frac{A_w}{A_s} \frac{1}{\epsilon_s} - 1 \right)} \right]}{c_w \rho_w \tau_w \frac{dT_w}{dt} + r} \right\} \sigma_{T_w} - \frac{\sigma_{T_w}}{T_{aw} - T_w} \right\rvert \approx \left\lvert - \frac{\sigma_{T_w}}{T_{aw} - T_w} \right\rvert$
T_s	$\left\lvert \frac{- \frac{\sigma_b T_s^3}{r} \left(\frac{1}{\left(\frac{1}{\epsilon_w} + \frac{A_w}{A_s} \frac{1}{\epsilon_s} - 1 \right)} \right) \sigma_{T_s}}{\frac{\rho_w \tau_w c_w \frac{dT_w}{dt}}{r} + 1} \right\rvert \approx 0$
ρ_o	$\left\lvert - \frac{\sigma_{\rho_o}}{\rho_o} \right\rvert$
T_o	$\left\lvert \frac{- \left[R.F. \left(1 - \frac{T_v}{T_o} \right) + \frac{T_v}{T_o} \right] \sigma_{T_o}}{T_{aw} - T_w} \right\rvert \approx \left\lvert \frac{-\sigma_{T_o}}{T_{aw} - T_w} \right\rvert$
V_o	$\left\lvert \left(\frac{0.4 R.F. V_o^2}{\frac{\gamma R}{T_{aw} - T_w} + 1} \right) \frac{\sigma_{V_o}}{V_o} \right\rvert \approx \left\lvert \frac{0.1 M_o \sigma_{V_o}}{T_{aw} - T_w} \right\rvert$
$\frac{dT_w}{dt}$	$\left\lvert \frac{\sigma_{dT_w/dt}}{\frac{dT_w}{dt} \left(1 + \frac{r}{\rho_w \tau_w c_w \frac{dT_w}{dt}} \right)} \right\rvert \approx \left\lvert \frac{\sigma_{dT_w/dt}}{dT_w/dt} \right\rvert$
τ_w	$\left\lvert \frac{\sigma_{\tau_w}}{\tau_w \left(1 + \frac{r}{\rho_w \tau_w c_w \frac{dT_w}{dt}} \right)} \right\rvert \approx \left\lvert \frac{\sigma_{\tau_w}}{\tau_w} \right\rvert$

Quantity	$\frac{\sigma C_H}{C_H}$ due to σ
$\frac{\rho_v}{\rho_o}$	$\left\lvert\frac{\sigma_{\rho_v/\rho_o}}{\rho_v/\rho_o}\right\rvert$
$\frac{V_v}{V_o}$	$\left\lvert\frac{\sigma_{V_v/V_o}}{V_v/V_o}\right\rvert$
$\frac{T_v}{T_o}$	$\left\lvert\frac{T_v(1 - R.F.)\sigma_{T_v/T_o}}{(T_{aw} - T_w)\frac{T_v}{T_o}}\right\rvert \approx \left\lvert\left(\frac{50}{T_{aw} - T_w}\right)\frac{\sigma_{T_v/T_o}}{T_v/T_o}\right\rvert$
ϵ_w	$\left\lvert\frac{\left\{\frac{\sigma_b \epsilon_w T_w^4 + \frac{\sigma_b}{\epsilon_w}\left(\frac{T_w^4 - T_s^4}{\left(\frac{1}{\epsilon_w} + \frac{A_w}{A_s}\frac{1}{\epsilon_s} - 1\right)^2}\right)}{r}\right\}\frac{\sigma\epsilon_w}{\epsilon_w}}{\frac{\rho_w \tau_w c_w \frac{dT_w}{dt}}{r} + 1}\right\rvert \approx \left\lvert\frac{\sigma\epsilon_w}{\epsilon_w}\right\rvert$

When values of the individual errors (see table at end of the appendix) are substituted in the approximate forms of the error terms and the results summed as in equation (A1), the following equation is obtained (for $M_o = 4$):

$$\frac{\sigma C_{H_{total}}}{C_H} \approx \left\{\frac{403}{(T_{aw} - T_w)^2} + \frac{1}{\left(\frac{dT_w}{dt}\right)^2} + 0.0022\right\}^{1/2}$$

As shown by this equation, the data become extremely inaccurate when $T_{aw} - T_w$ and $\frac{dT_w}{dt} \rightarrow 0$; this effect is compounded since both these terms

go to zero at about the same time. A comparison of this equation with equation (A1) computed using the complete error terms is shown in figure 10.

As can be seen from the upper part of figure 10, the percentage error where the $T_{aw} - T_w$ difference is over 100° R is of the order of 20 percent or less. The percentage errors in this upper plot have been used to calculate values of $\sigma_{C_{H_{total}}}$ which have been added and subtracted from the data and the results presented as a shaded area in the lower plot. It seems apparent from the comparison of the shaded band and the theoretical curve that nowhere are the data in significant disagreement with the theoretical calculations. This is more apparent when it is realized that the values from theoretical calculations should be even higher than shown here due to the presence of laminar regions on the body. (See fig. 12(a).) This conclusion applies to the data of the remaining stations as well.

Estimation of Errors of Individual Measurements

Wall and shield temperatures.- Assuming the absence of systematic errors in the temperature measurements permits the random errors to be divided into two classes. In one group, the errors are such that they do not vary rapidly with time - for example, calibration errors and slow telemeter drifts. The other type exhibits itself in the data as random scatter with time and is probably due in great part to the errors involved in the recording and reading of the data.

This latter type of error can be evaluated from the data when dT/dt is less than about 25° per second. Such evaluation gives $\sigma_T = 5°$. This error is important only in flight conditions which give high rates of temperature increase but even there it is overshadowed by the first type of error, as will be shown.

The error of the first kind can be evaluated only by comparisons of tests made under identical conditions with different telemeters. Since this comparison has not been made (in fact it would prove very difficult to make in the temperature ranges of interest because of the difficulty of knowing or reproducing the conditions), it is necessary for a value to be assumed on the basis of experience with past measurements. In general, the accuracy of telemeter data of all kinds has been roughly estimated as 1 to 2 percent of the full-scale range of the instrument used. Previous tests using temperature equipment similar to that used on the present tests have indicated that temperature data are at least as good and are probably better than the larger of these figures. Thus for the purposes of this evaluation a figure of 1 percent of the full-scale value will be used and this estimate gives a value of σ_T of 20°.

Error in ρ_o and T_o.- Errors involved in the determination of both ρ_o and T_o are a combination of three independent factors:

(1) Error in the measured altitude of the model

(2) Error in the calculated altitude of the radiosonde

(3) Error in the measurement of the quantities ρ_o and T_o

In the altitude range of the present tests the estimated accuracy of the two altitude measurements together with the rates of change of ρ_o and T_o with altitude give errors in these quantities of $\sigma_{\rho_o} = 0.006$ and $\sigma_{T_o} = 0.2^\circ$. Unpublished NACA tests give values of $\sigma_{\rho_o} = 0.0083$ and $\sigma_{T_o} = 0.9^\circ$ for the radiosonde instrument error in the altitude range below 50,000 feet. Since these errors are independent, they can be combined by the equation $\sigma_{total} = \sqrt{\sigma_a^2 + \sigma_b^2}$. This gives the total σ as follows:

$$\sigma_{\rho_o} = 0.013\rho_o \quad \text{and} \quad \sigma_{T_o} = 1^\circ \text{ F}$$

Error in V_o.- In the altitude range considered the major error in velocity measurement is due to the inaccuracies in the measurement of wind velocity. Since the wind velocity is not measured at the time and place of the model, any accuracy which may be quoted is open to some doubt. However, consideration of accuracy of the actual measurements used to obtain the wind velocity as it affects the radiosonde balloon leads to a figure of $\sigma_{V_o} = 4$ feet per second.

Error in $\frac{dT_w}{dt}$.- If the measured temperatures are assumed correct, errors in $\frac{dT_w}{dt}$ are caused by inaccuracies in the fairing of the temperature data and in the reading of the slopes of the faired curves. An inspection of the scatter of such readings leads to a figure of $\sigma_{dT_w/dt} = 1^\circ$ per second for the faired results. This value seems to include both types of error since an average error of $\frac{dT_w}{dt} = 1^\circ$ per second was obtained by integrating the slope curves and comparing the resulting temperatures with the original temperature curve for the data of a typical station.

Errors in $\frac{\rho_v}{\rho_o}$, $\frac{V_v}{V_o}$, and $\frac{T_v}{T_o}$.- Errors in the quantities ρ_v/ρ_o, V_v/V_o, and T_v/T_o may all be referred to error in the calculation of the pressures over the body. While this error will be a function of the computation methods used, it can be seen from the comparison of the various methods with the results of the method of characteristics in reference 15 that a value of $\sigma_{c_p} = 0.05c_p$ is not unreasonably low. This comparison of course includes the assumption that the method of characteristics gives correct values, and this assumption has been shown to be a good one except for flight conditions where the boundary layer might be expected to appreciably affect the flow contour about the body. This latter condition should not exist in the present tests. Using the value $\sigma_{c_p} = 0.05c_p$ values of $\sigma_{\rho_v/\rho_o, V_v/V_o, T_v/T_o}$ can be obtained as functions of p_v/p_o. This value is, for any particular model, a function of Mach number and body station. However, for the present body and Mach numbers, p_v/p_o is small and leads to values of

$$\sigma_{\rho_v/\rho_o, V_v/V_o, T_v/T_o} \leq 0.01 \frac{\rho_v}{\rho_o}, \frac{V_v}{V_o}, \frac{T_v}{T_o}$$

Error in τ_w.- The accuracy of the measurement of the wall thickness is estimated to be about 0.001 inch. For the wall thickness of the present model this estimate leads to a value of $\sigma_{\tau_w} \approx 0.03\tau_w$.

Error in ϵ_w.- The error in this quantity was estimated from the apparent scatter in the data of its measured values and is $\sigma_{\epsilon_w} = 0.02$.

Error in c_{p_v}, ρ_w, σ_b, c_w, and R.F..- The values of c_{p_v}, ρ_w, σ_b, c_w, and R.F. have been assumed to be constants in which no error appears. Although it is assumed that c_w is known absolutely, it is a quantity which varies with T_w and the error attributable to this fact appears in the error for T_w. While c_{p_v} is a function of T_v, T_v varies so little that any error due to an error in T_v is quite negligible.

In the presentation of the data the recovery factor R.F. is assumed to be equal to $Pr^{1/3}$ and $Pr^{1/2}$ for turbulent and laminar boundary layers, respectively, and thus the errors are assumed 0. It

should be noted, however, that the equation for the error in C_H due to R.F. error,

$$\left(\frac{\sigma_{C_H}}{C_H}\right)_{R.F.} = \frac{T_{aw} - T_v}{T_{aw} - T_w} \frac{\sigma_{R.F.}}{R.F.}$$

shows that small errors in this quantity can lead to quite large errors in C_H when $T_{aw} - T_w \rightarrow 0$.

The values of the errors used in obtaining the data of figure 10 are presented in tabular form as follows:

Quantity	σ
T_w	20° R
T_s	20° R
ρ_o	$0.013\rho_o$
T_o	1° R
V_o	4 fps
dT_w/dt	1° per sec
τ_w	$0.03\tau_w$
$\frac{\rho_v}{\rho_o}, \frac{T_v}{T_o}, \frac{V_v}{V_o}$	$\leqq 0.01 \frac{\rho_v}{\rho_o}, \frac{T_v}{T_o}, \frac{V_v}{V_o}$
ϵ_w	0.02

REFERENCES

1. Piland, Robert O.: Drag Measurements on a 1/6-Scale, Finless, Sting-Mounted NACA RM-10 Missile in Flight at Mach Numbers From 1.1 to 4.04 Showing Some Reynolds Number and Heating Effects. NACA RM L54H09, 1954.

2. Chauvin, Leo T., and Maloney, Joseph P.: Turbulent Convective Heat-Transfer Coefficients Measured From Flight Tests of Four Research Models (NACA RM-10) at Mach Numbers From 1.0 to 3.6. NACA RM L54L15, 1955.

3. Chauvin, Leo T., and de Moraes, Carlos A.: Correlation of Supersonic Convective Heat-Transfer Coefficients From Measurements of the Skin Temperature of a Parabolic Body of Revolution (NACA RM-10). NACA RM L51A18, 1951.

4. Eckert, E. R. G. (With Appendix by Robert M. Drake, Jr.): Introduction to the Transfer of Heat and Mass. First ed., McGraw-Hill Book Co., Inc., 1950.

5. Ginnings, Defoe C., and Thomas, Eugenia: The Electrical Resistance and Total Radiant Emittance of Inconel in the Range 0° to 1000° C. NBS Rep. 4111 (NACA Contract S54-52), Nat. Bur. Standards. May 1955.

6. Keenan, Joseph H., and Kaye, Joseph: Thermodynamic Properties of Air Including Polytropic Functions. John Wiley & Sons, Inc., 1945.

7. Kaye, Joseph: Survey of Friction Coefficients, Recovery Factors, and Heat-Transfer Coefficients for Supersonic Flow. Jour. Aero. Sci., vol. 21, no. 2, Feb. 1954, pp. 117-129.

8. Jones, Robert T., and Margolis, Kenneth: Flow Over a Slender Body of Revolution at Supersonic Velocities. NACA TN 1081, 1946.

9. Van Driest, E. R.: The Turbulent Boundary Layer for Compressible Fluids on a Flat Plate With Heat Transfer. Rep. No. AL-997, North American Aviation, Inc., Jan. 27, 1950.

10. Van Driest, E. R.: Investigation of Laminar Boundary Layer in Compressible Fluids Using the Crocco Method. NACA TN 2597, 1952.

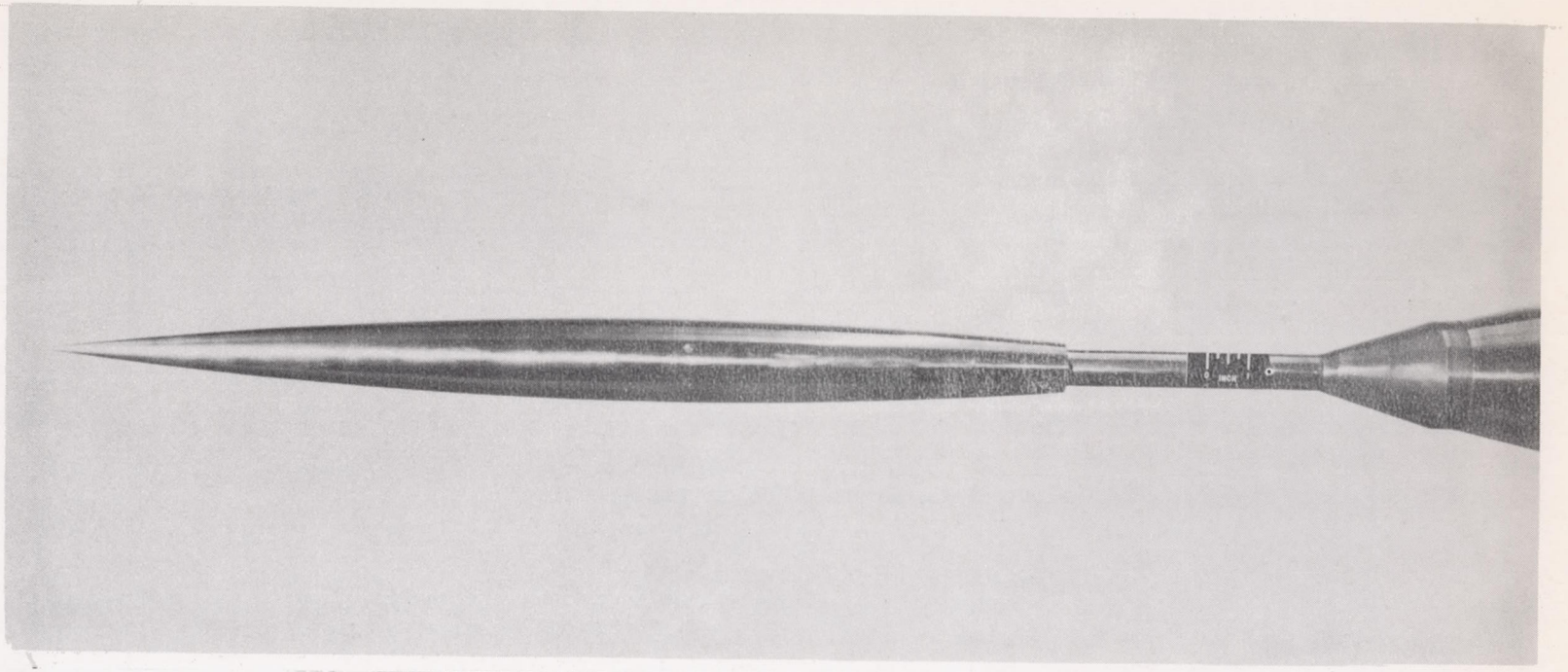
11. Van Driest, E. R.: Turbulent Boundary Layer on a Cone in a Supersonic Flow at Zero Angle of Attack. Jour. Aero. Sci., vol. 19, no. 1, Jan. 1952, pp. 55-57, 72.

12. Eckert, Ernst R. G.: Survey on Heat Transfer at High Speeds. WADC Technical Report 54-70, Wright Air Dev. Center, U. S. Air Force, Apr. 1954.

13. Van Driest, E. R.: Calculation of the Stability of the Laminar Boundary Layer in a Compressible Fluid on a Flat Plate With Heat Transfer. Jour. Aero. Sci., vol. 19, no. 12, Dec. 1952, pp. 801-812.

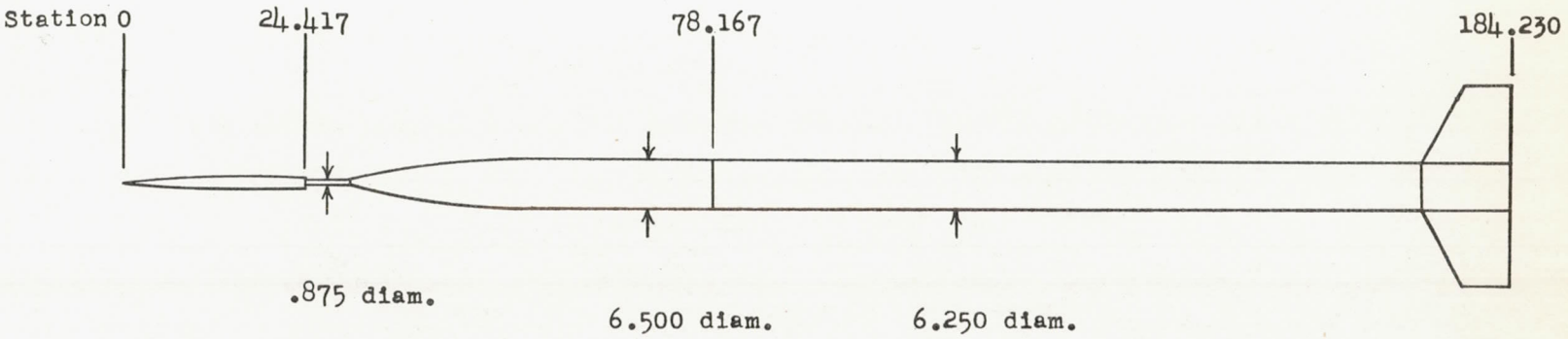
14. Eshbach, Ovid W.: Handbook of Engineering Fundamentals. Second ed., John Wiley & Sons, Inc., 1954.

15. Ehret, Dorris M.: Accuracy of Approximate Methods for Predicting Pressures on Pointed Nonlifting Bodies of Revolution in Supersonic Flow, NACA TN 2764, 1952.

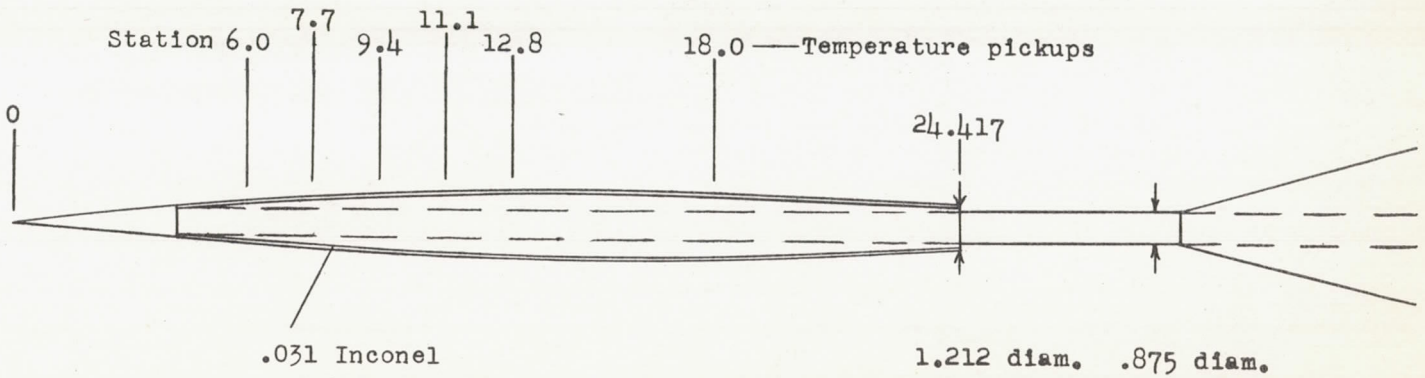


L-87845

Figure 1.- Photograph of 1/6 scale, sting-mounted NACA RM-10 test model.

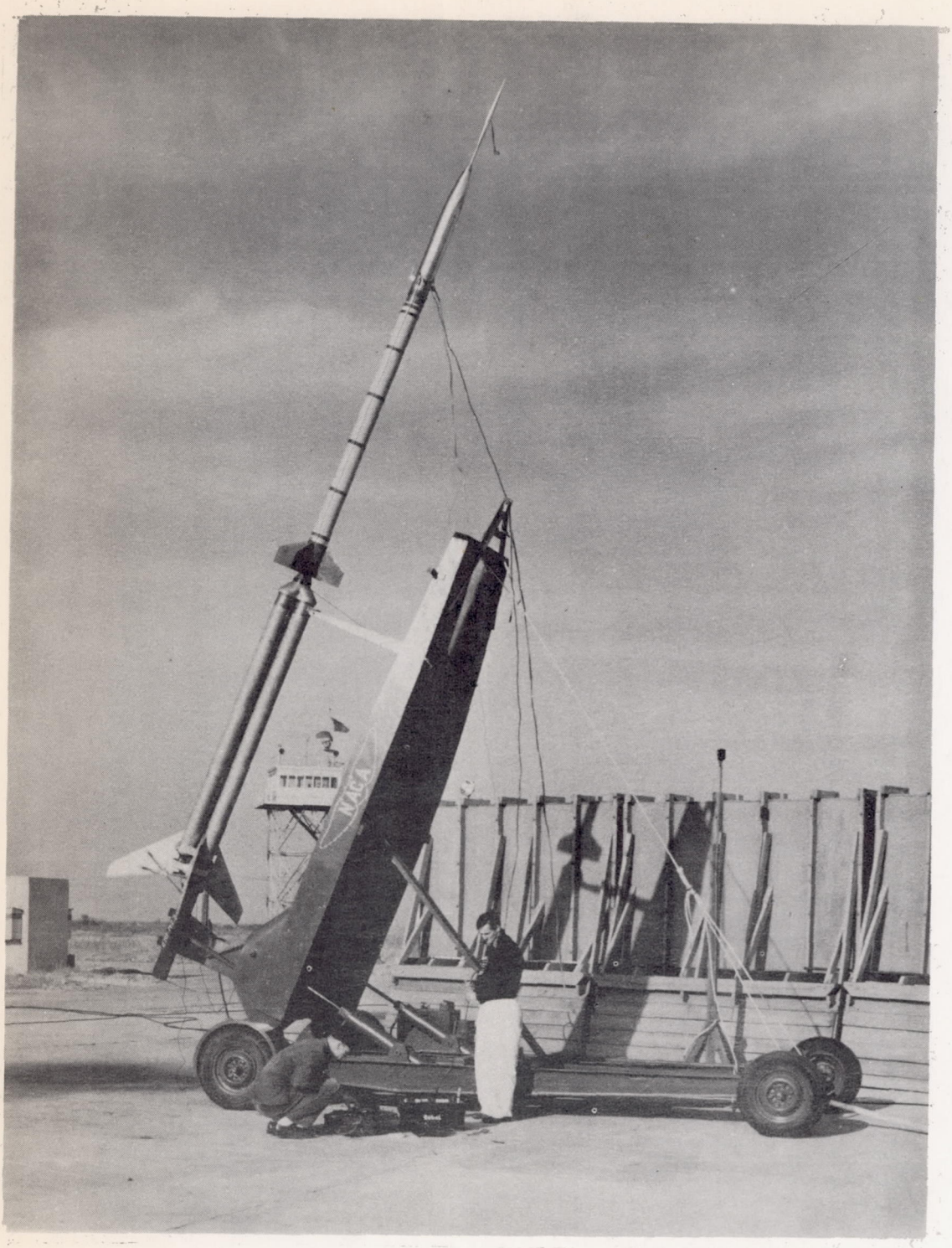


(a) Model mounted on carrier body.



(b) Model alone.

Figure 2.- Sketches of test model and carrier vehicle and of model alone showing temperature pick-up stations. (All dimensions are in inches.)



L-88158

Figure 3.- Model with booster on launcher ready for firing.

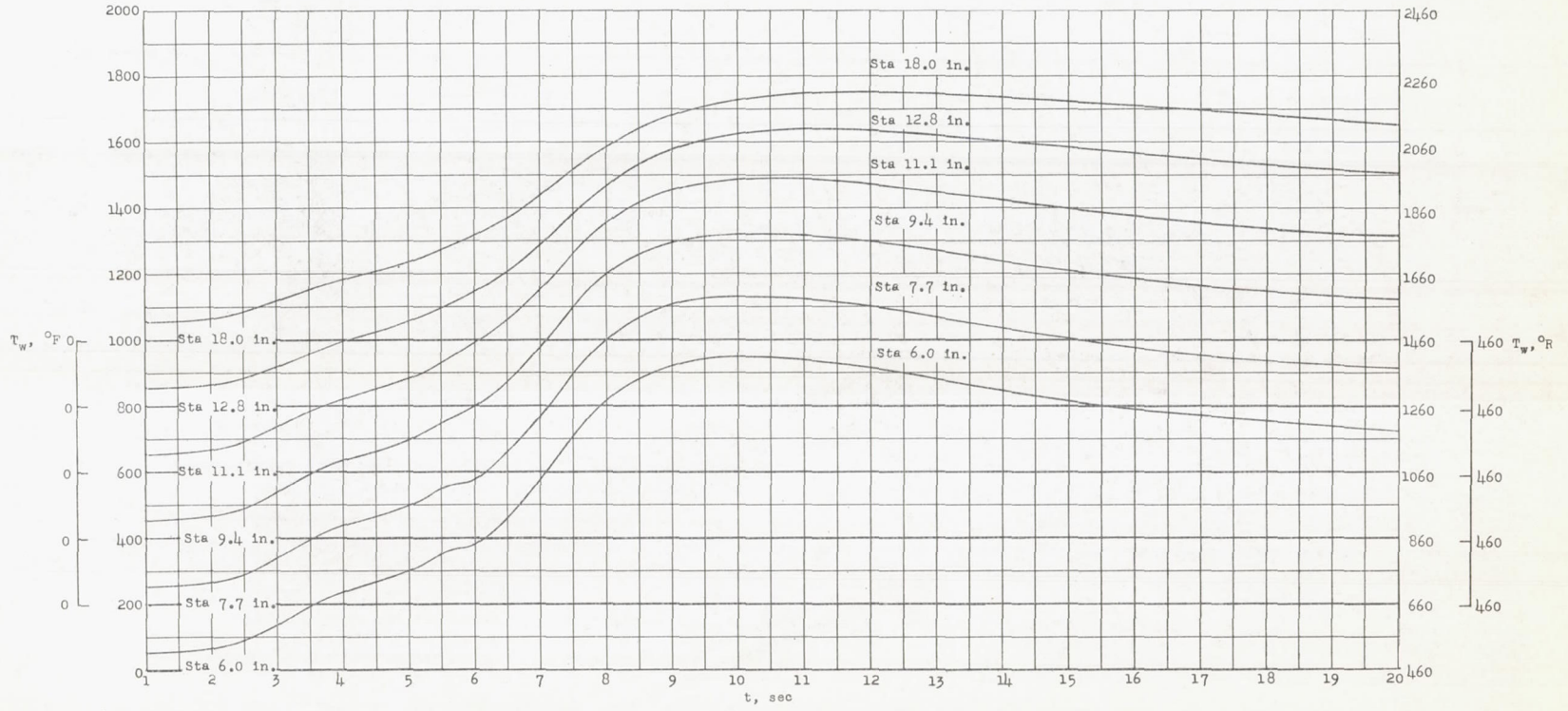


Figure 4.- Skin temperatures measured for six stations.

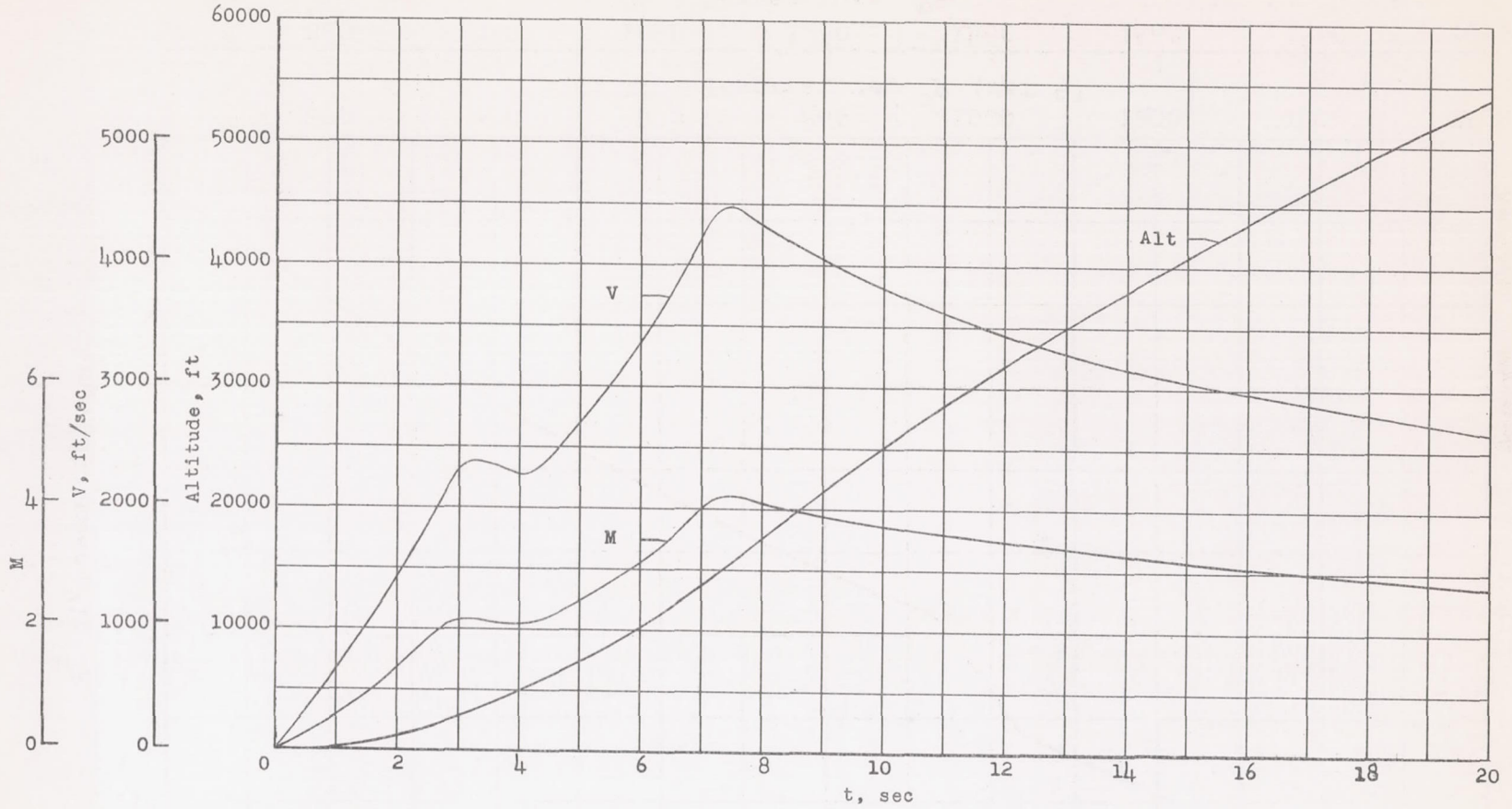


Figure 5.- Measured flight conditions.

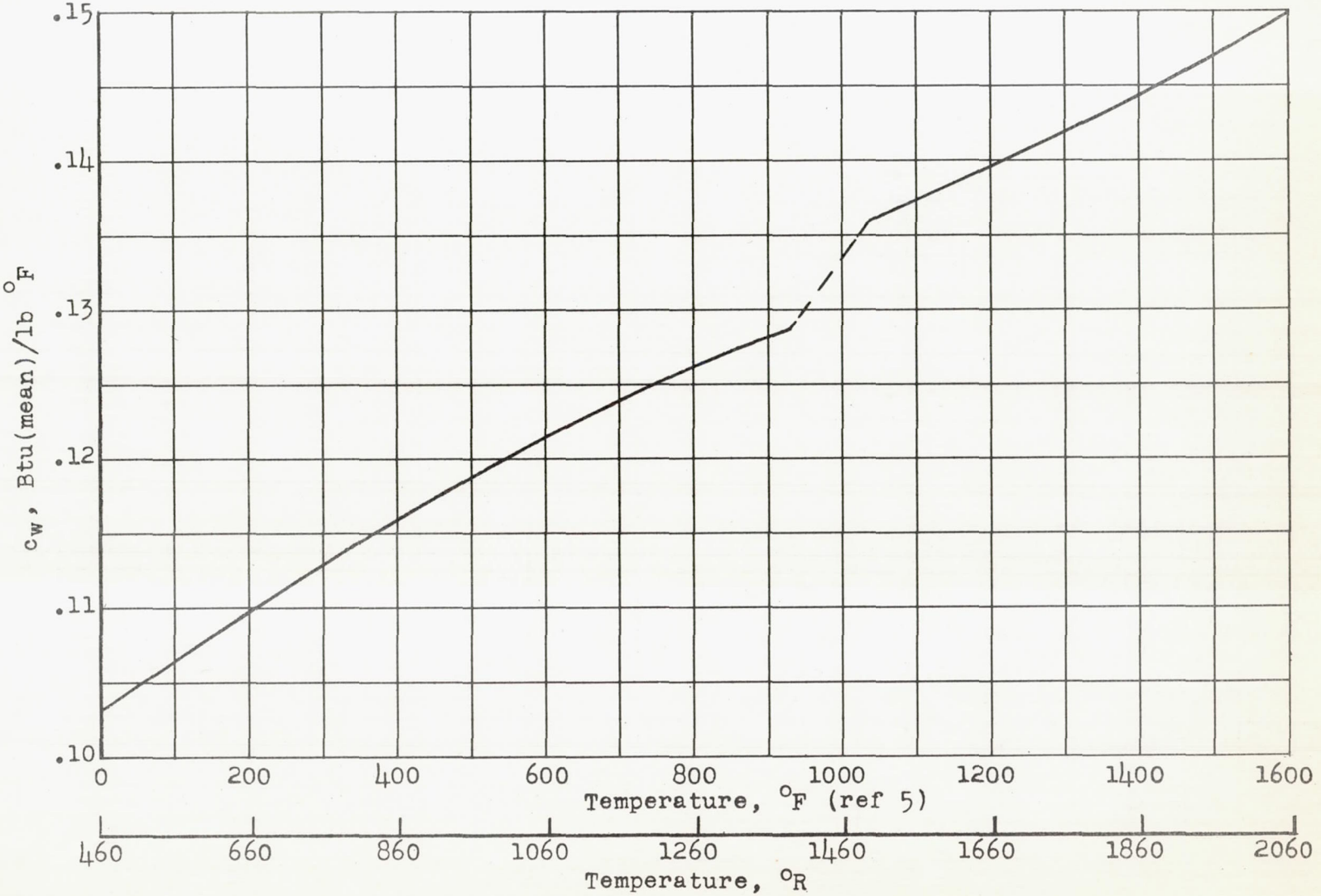


Figure 6.- Instantaneous specific heat of Inconel.

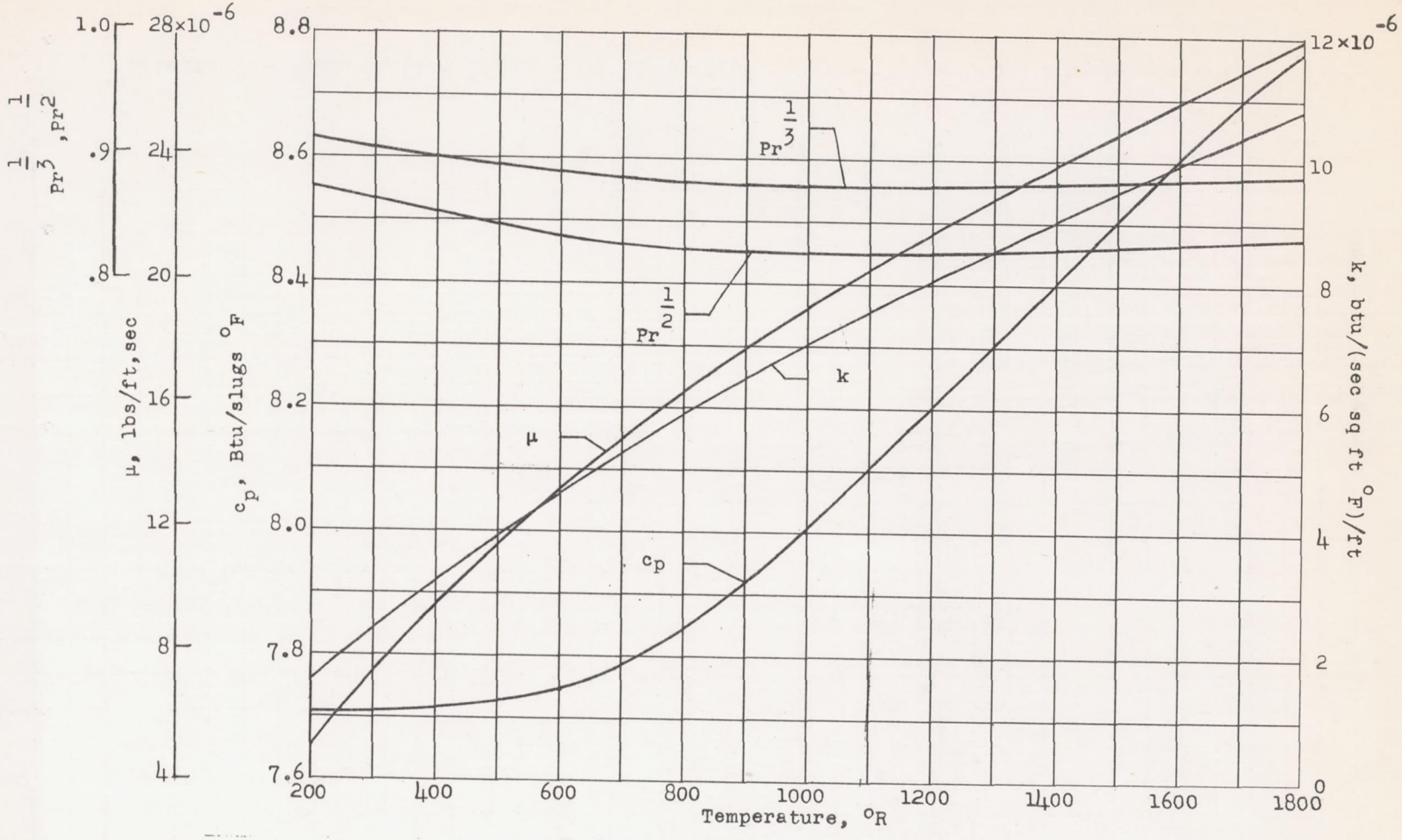


Figure 7.- Thermal properties of air, reference 6.

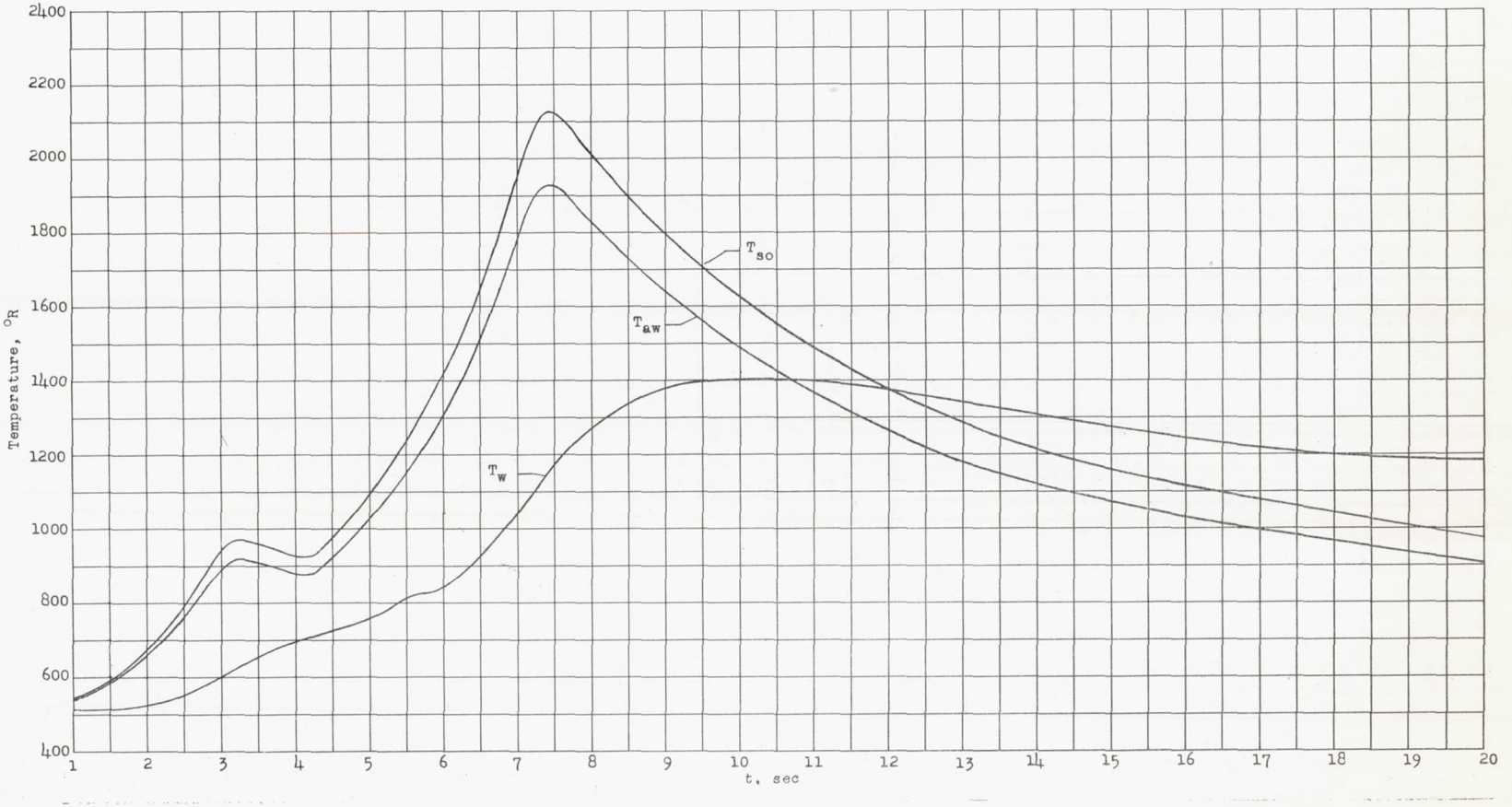


Figure 8.- Typical time history of stagnation, adiabatic, and skin temperatures.

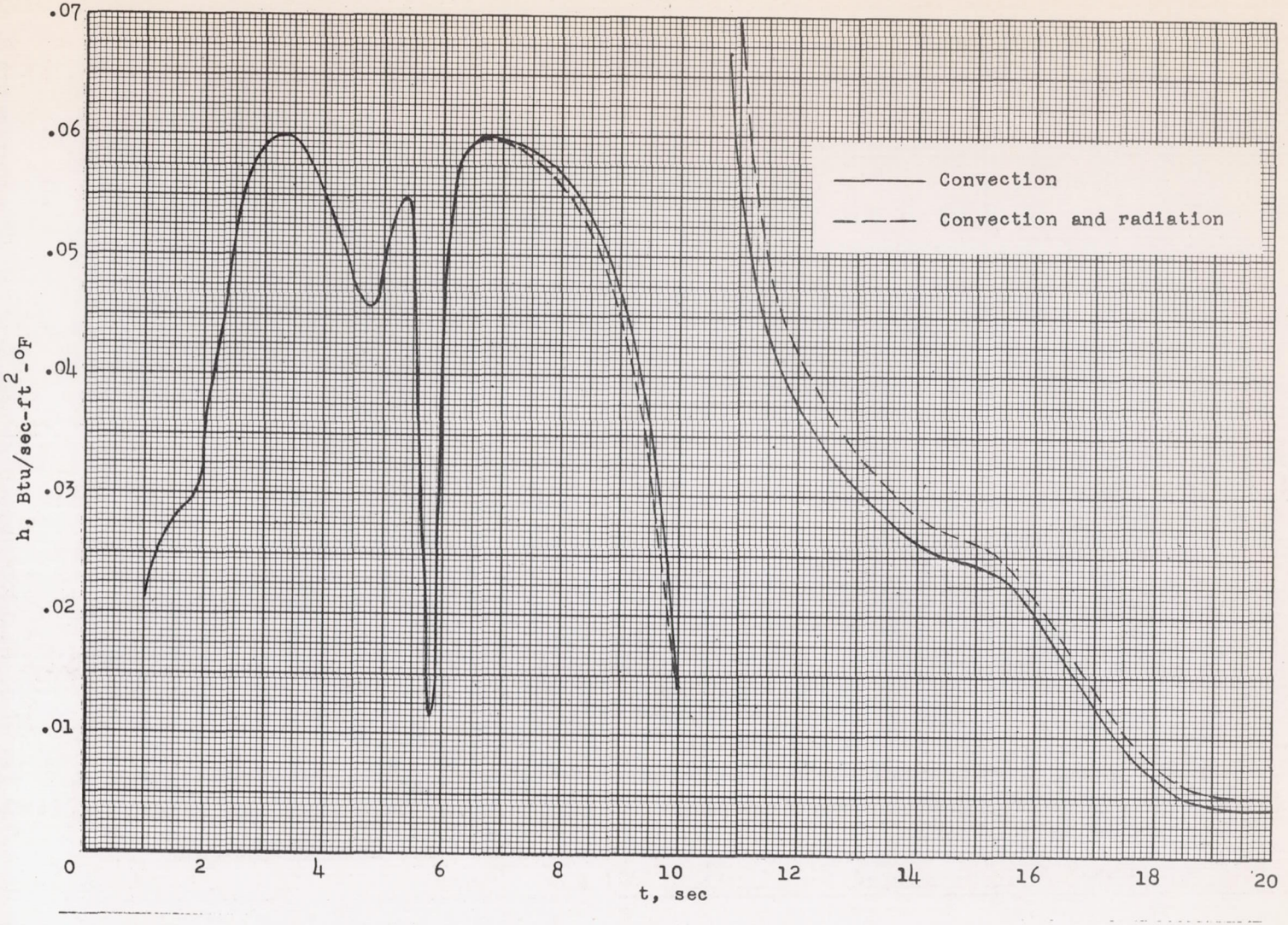


Figure 9.- Heat-transfer coefficients for station 7.7 inches showing the effects of radiation and convection.

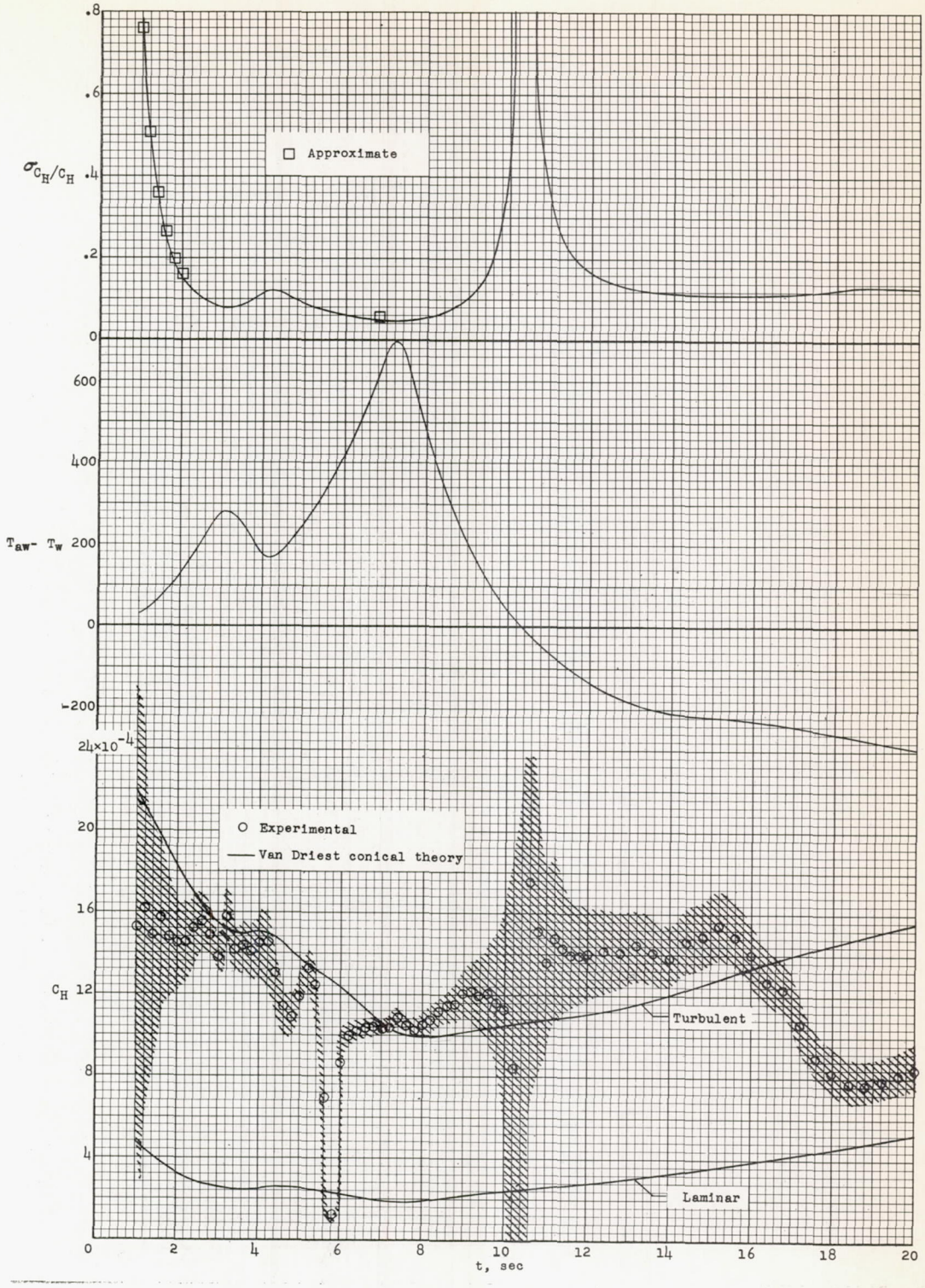


Figure 10.- The ratio of Stanton number probable error to experimental Stanton number, heating potential and accuracy band for experimental Stanton numbers varying with time at station 6.

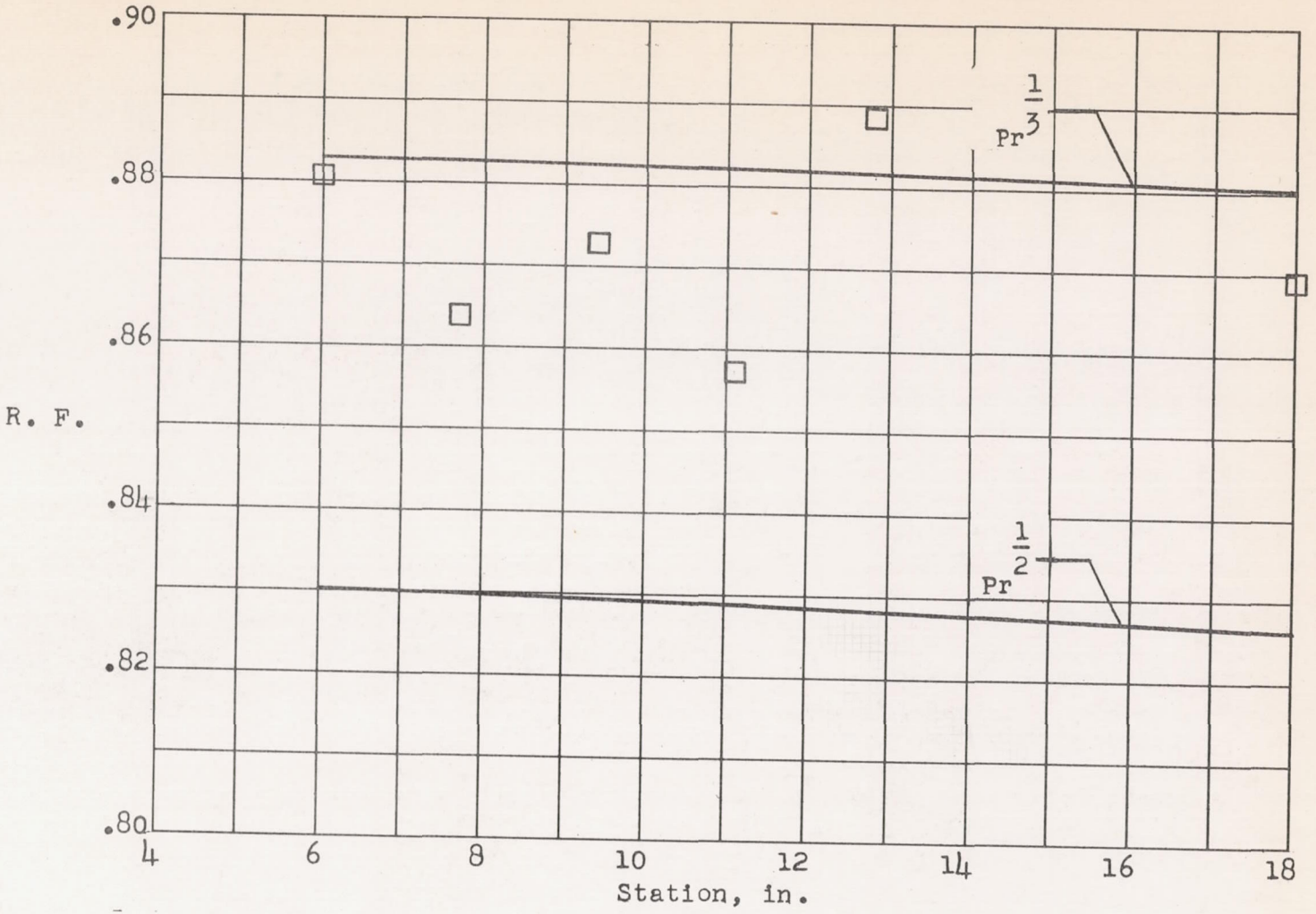
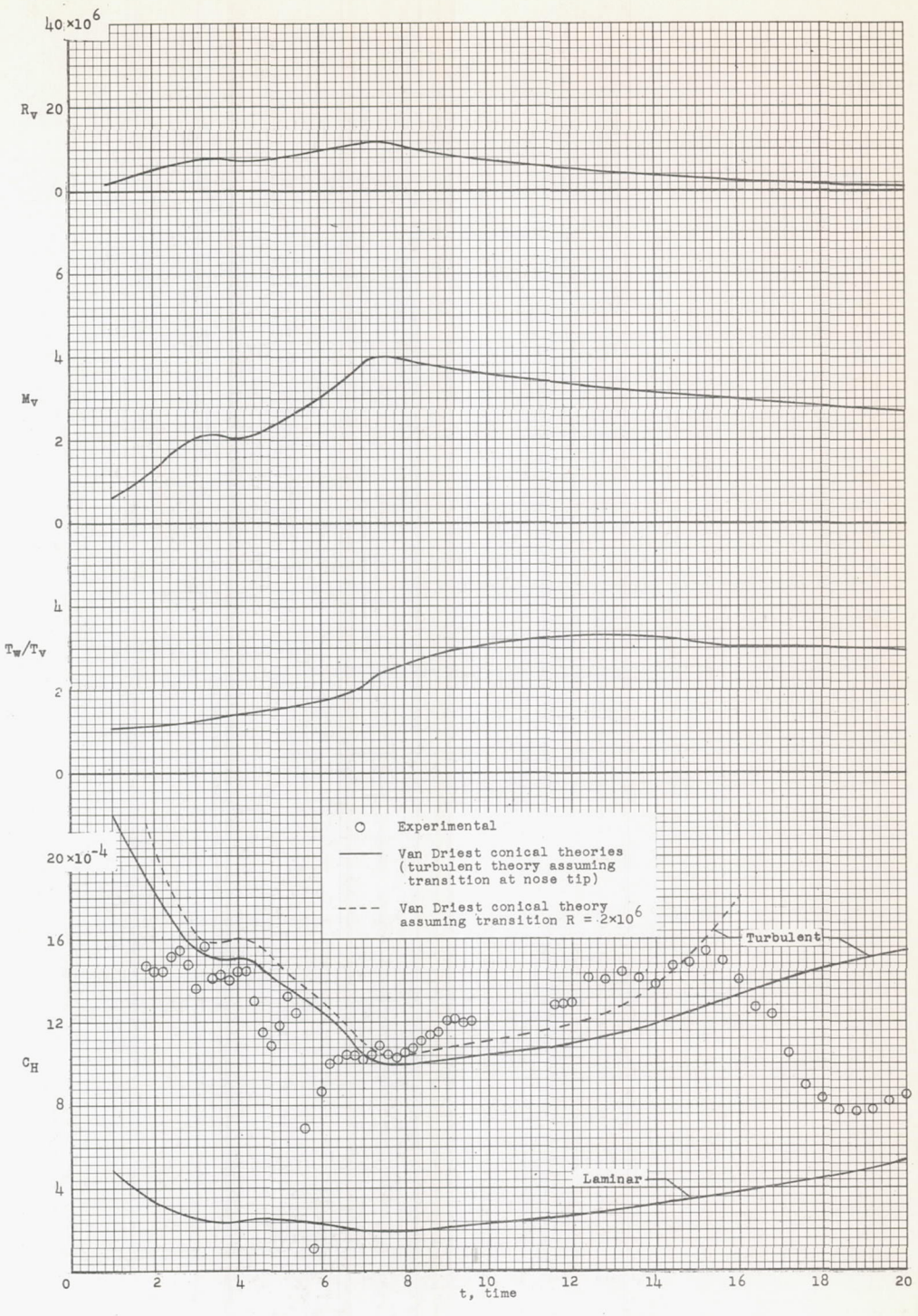
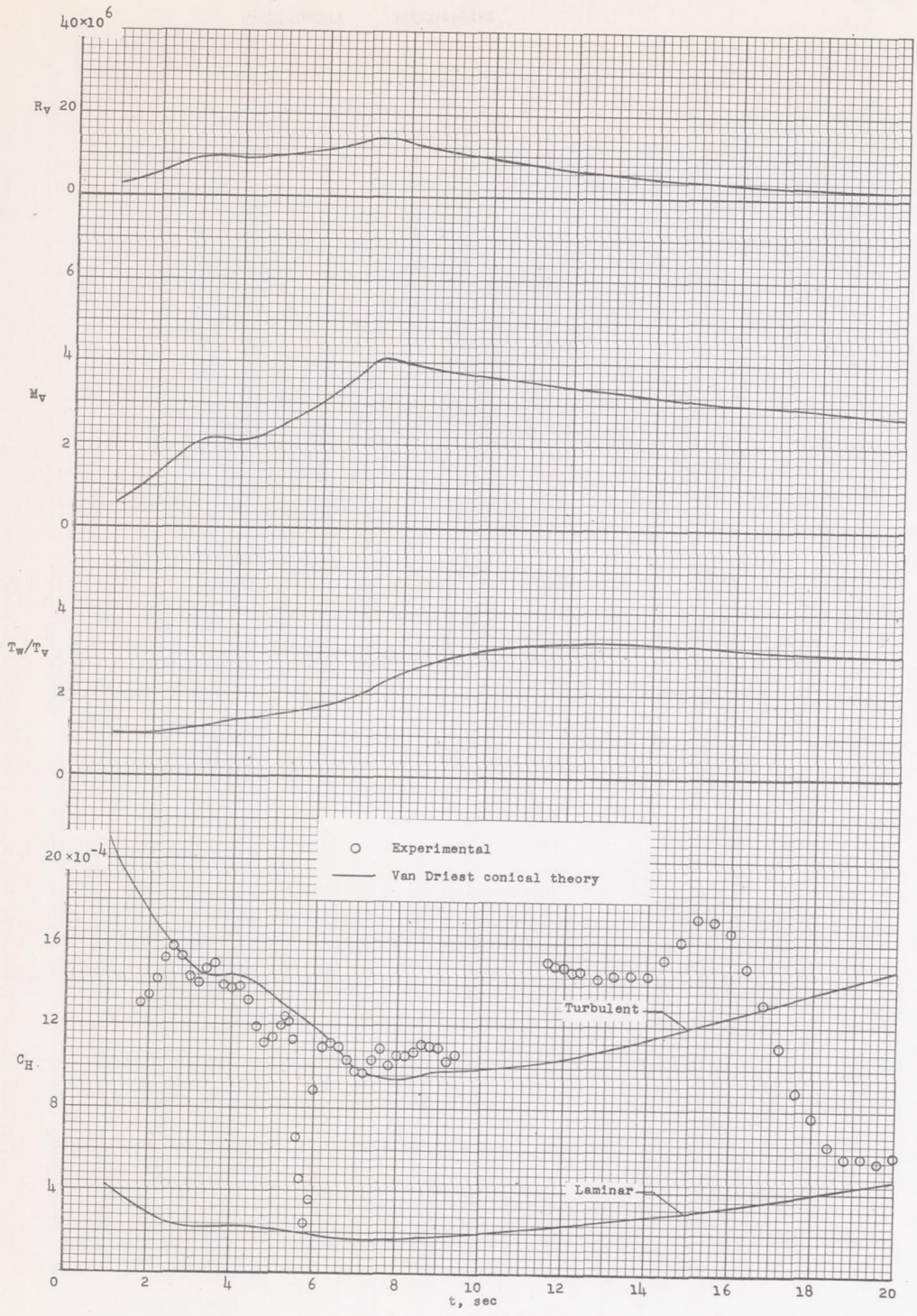


Figure 11.- Variation of measured and theoretical recovery factors with station. $Pr^{1/3}$ and $Pr^{1/2}$ are plotted for the times used in obtaining the measured recovery factors.



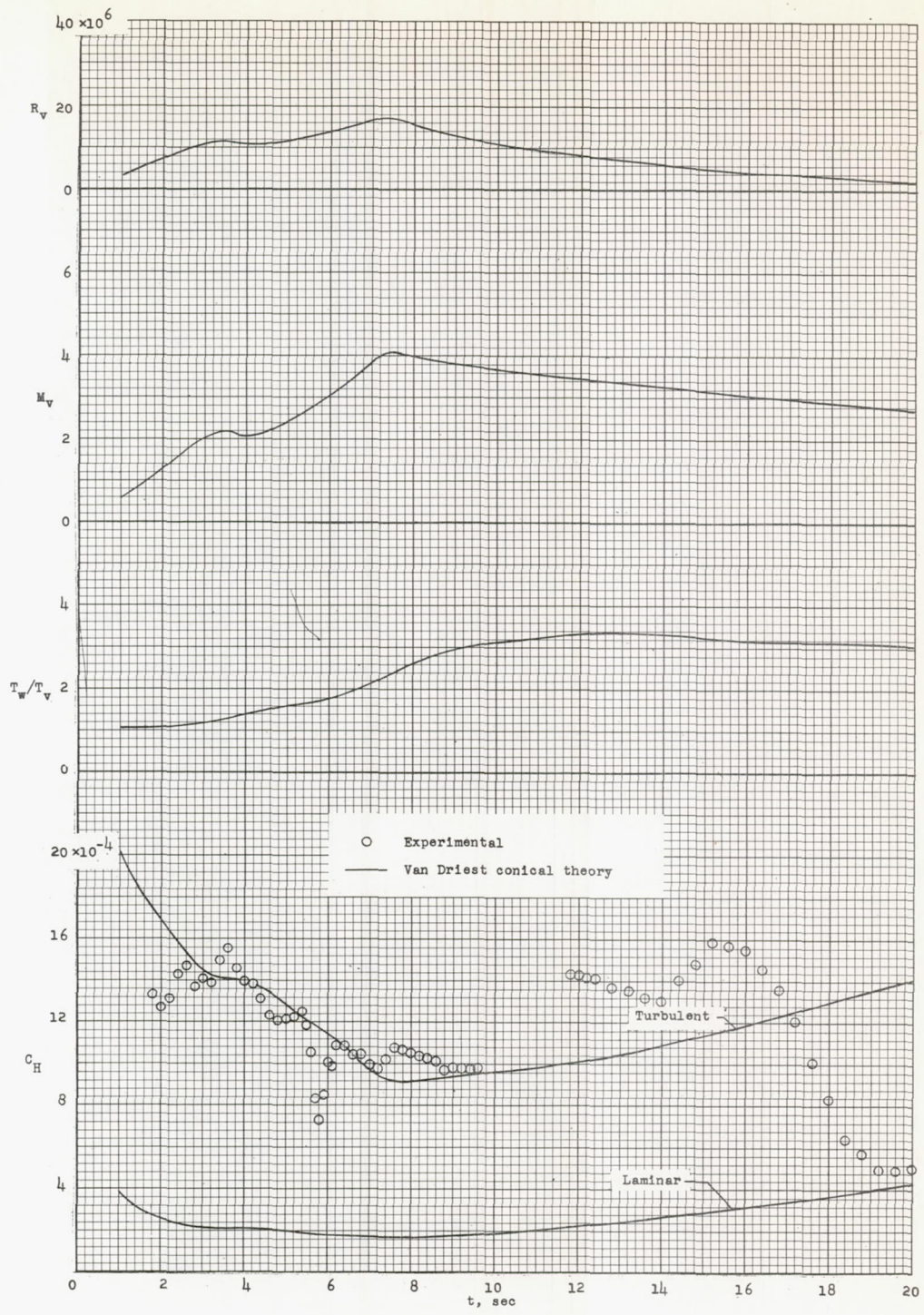
(a) Station 6.0 inches.

Figure 12.- Stanton number C_H and the quantities affecting Stanton number for the six temperature stations.



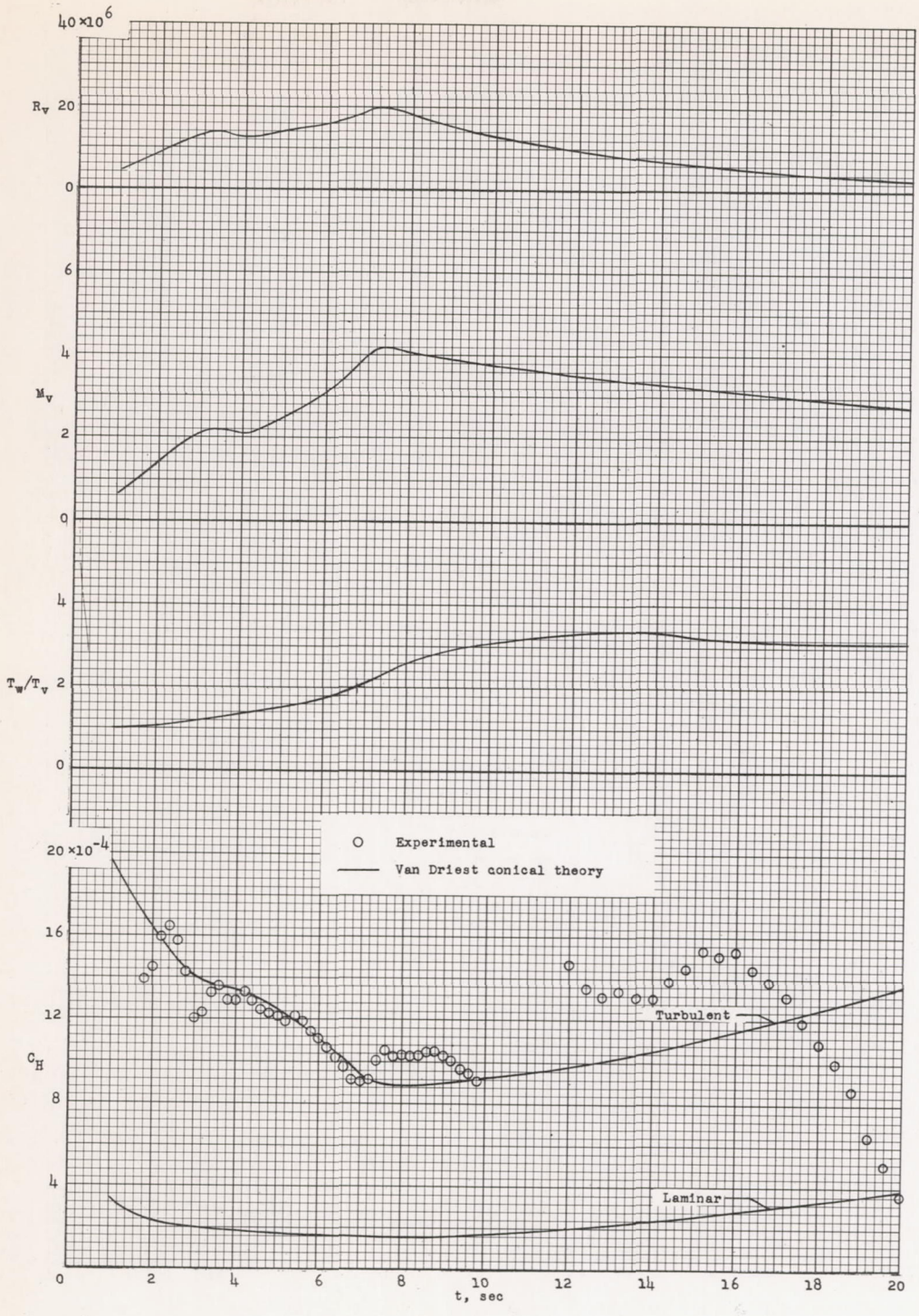
(b) Station 7.7 inches.

Figure 12.- Continued.



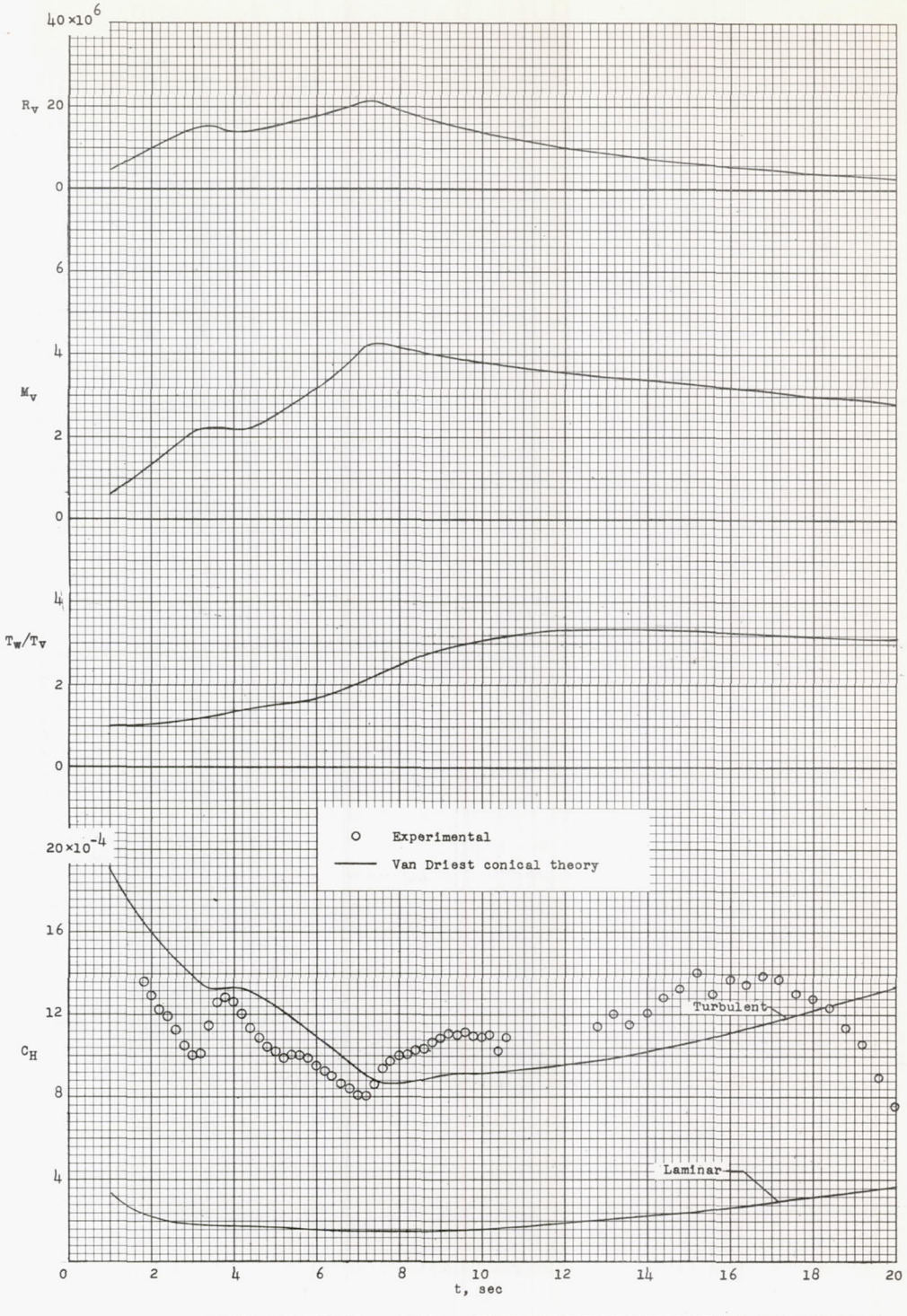
(c) Station 9.4 inches.

Figure 12.- Continued.



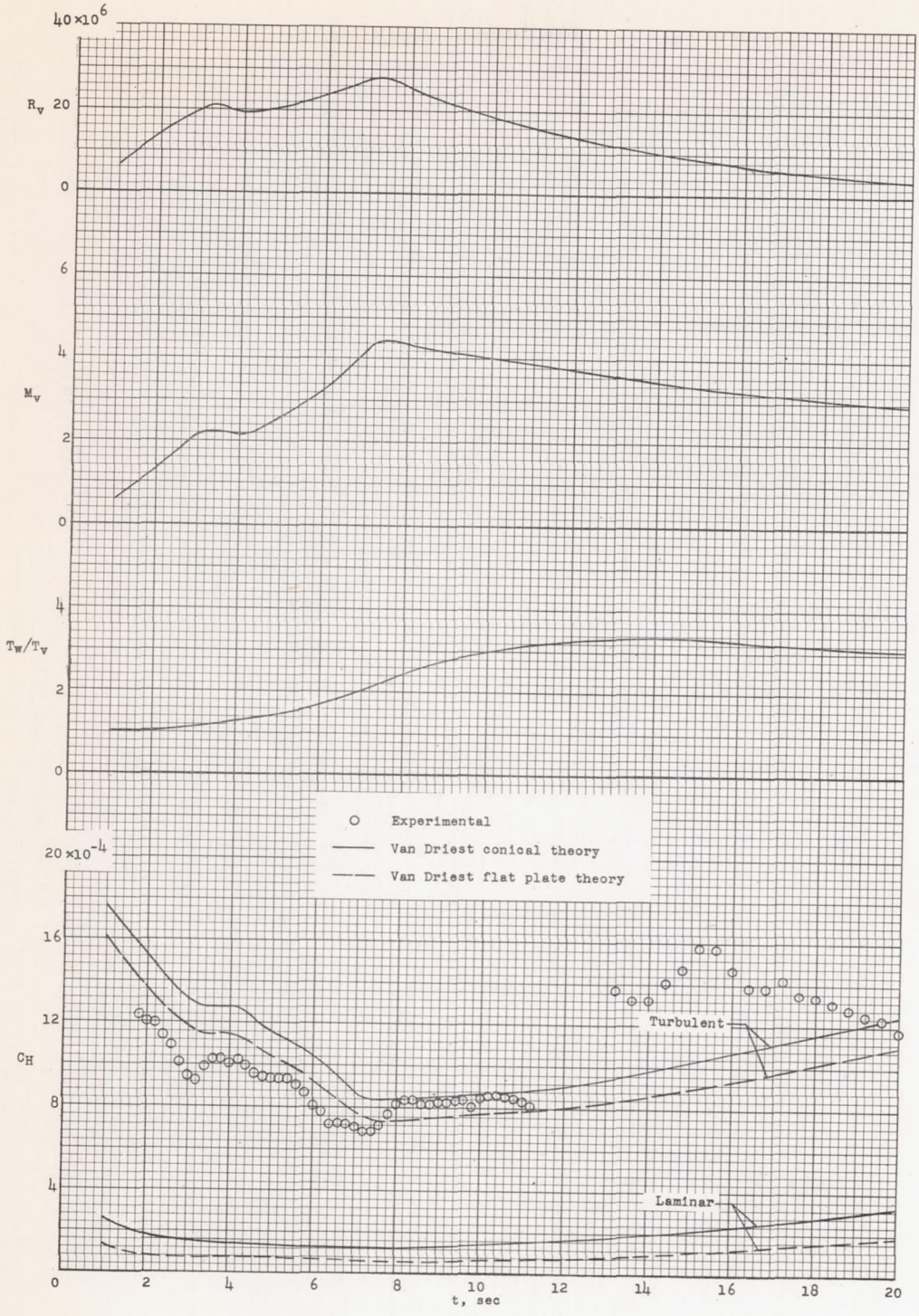
(d) Station 11.1 inches.

Figure 12.- Continued.



(e) Station 12.8 inches.

Figure 12.- Continued.



(f) Station 18.0 inches.

Figure 12.- Concluded.

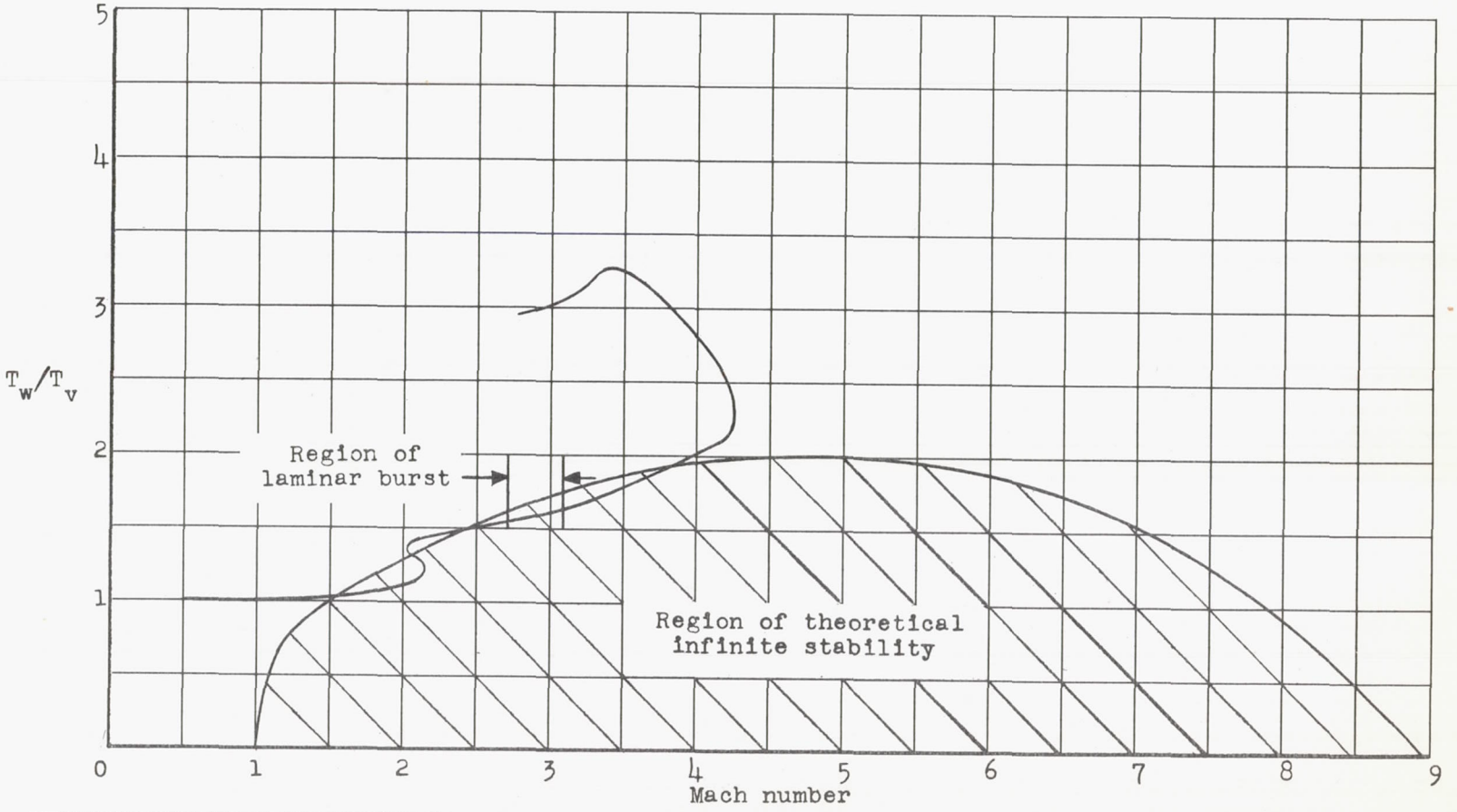
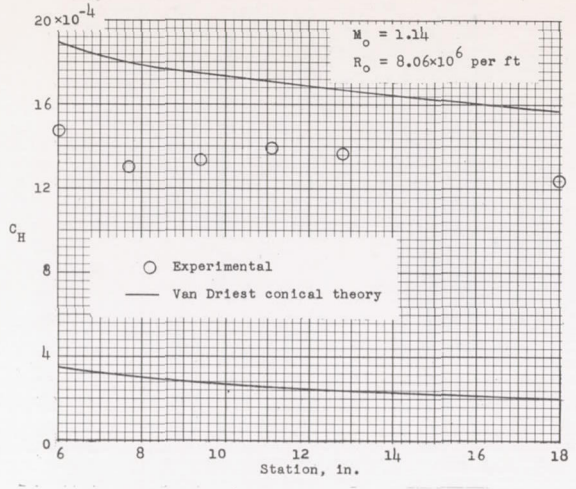
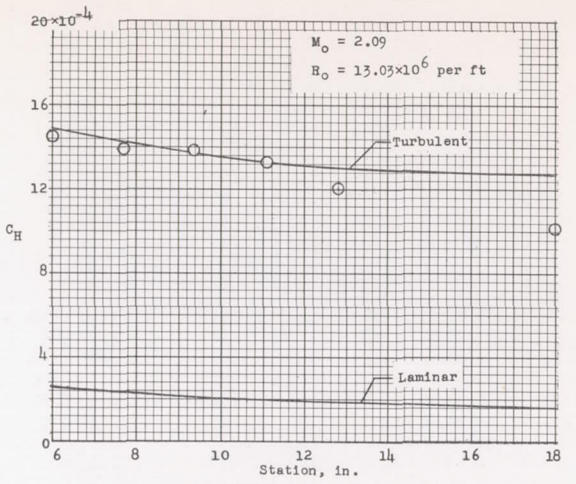


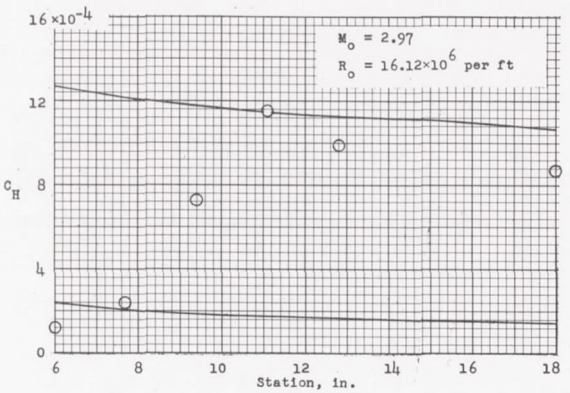
Figure 13.- Comparison of flight conditions with conditions for infinite stability of the laminar boundary layer.



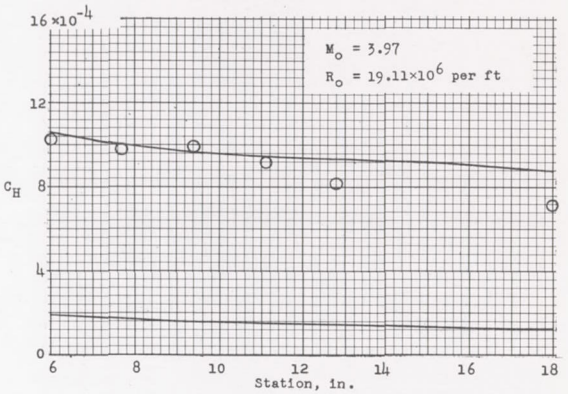
(a) 1.8 seconds.



(b) 4.2 seconds.

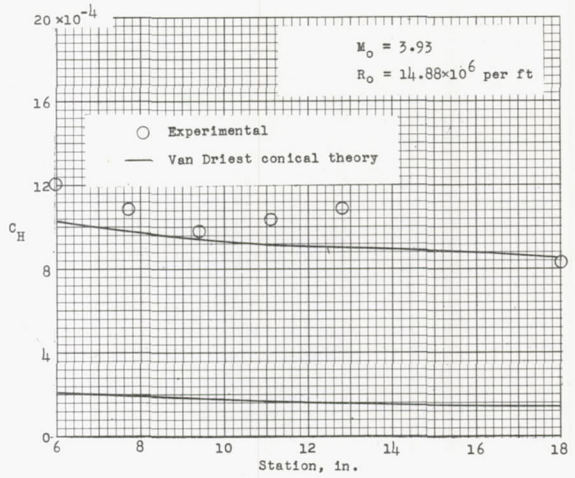


(c) 5.8 seconds.

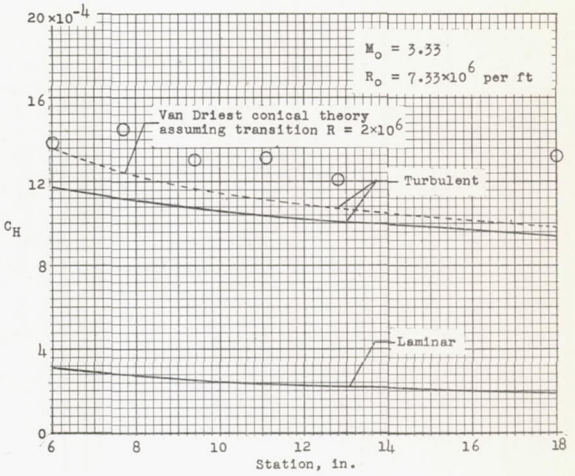


(d) 7.0 seconds.

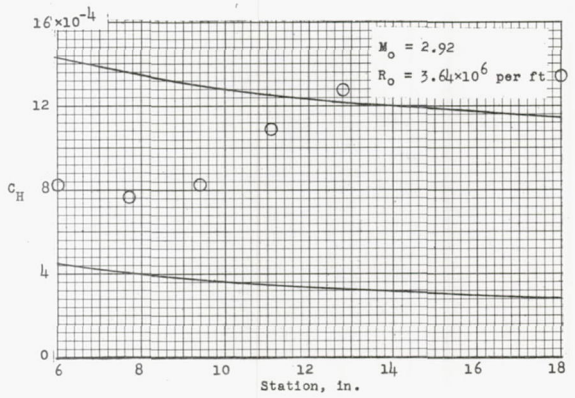
Figure 14.- Stanton number varying with stations along the body for a given time.



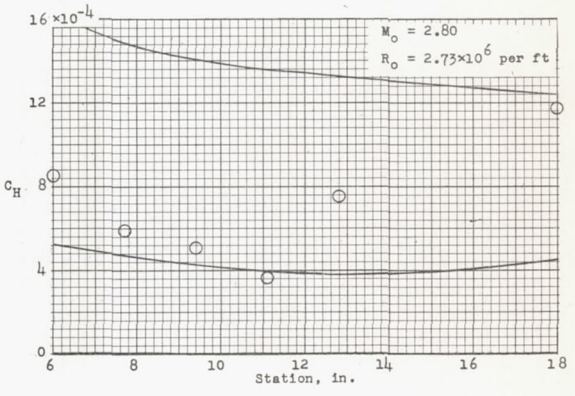
(e) 9.0 seconds.



(f) 14.0 seconds.



(g) 18.0 seconds.



(h) 20.0 seconds.

Figure 14.- Concluded.